The role of topography and the north Indian monsoon on mean monthly climate interpolation within the Himalayan Kingdom of Bhutan

Stewart, Stephen B[1,3], Choden, Kunzang[2], Fedrigo, Melissa[3,4], Roxburgh, Stephen H[3], Keenan, Rodney[2], Nitschke, Craig R[1].

1 School of Ecosystem and Forest Sciences, Faculty of Science, University of Melbourne, 500 Yarra Boulevard, Richmond, Victoria, 3121, Australia.

2 School of Ecosystem and Forest Sciences, Faculty of Science, University of Melbourne, Grattan Street, Parkville, Victoria, 3010, Australia.

3 CSIRO Land and Water, GPO Box 1700, Canberra, Australian Capital Territory, 2601, Australia.

4 Centre for Tropical Environmental and Sustainability Studies, James Cook University, PO Box 6811, Cairns, Queensland, 4870, Australia.

Corresponding author:

Stephen Stewart

500 Yarra Boulevard, Richmond, VIC, 3121, Australia

stephen.stewart85@gmail.com

+61 402 766 147

Abstract

Spatial climate datasets currently available for Bhutan are limited by weather station data availability, spatial resolution, or interpolation methodology. This paper presents new datasets for monthly maximum temperature, minimum temperature, precipitation and vapour pressure climate normals interpolated for the 1986-2015 reference period using trivariate smoothing splines. The inclusion of standardised day time Moderate Resolution Imaging Spectroradiometer (MODIS) land surface temperature (LST) values as partial spline dependencies reduced cross validated RMSE for maximum temperature by up to 16.0% and was most effective between March and September. Using both a topographic index of relative elevation and standardised night time MODIS LST values as partial spline dependencies reduced monthly mean minimum temperature RMSE by up to 23.4%. Neither variable was effective for minimum temperature interpolation between June and September. High humidity, extensive cloud cover and heavy precipitation occur during these months, which are likely to suppress the formation of temperature inversions that typically form under clear, calm conditions. These new temperature and precipitation surfaces show distinct differences from the WorldClim and CRU CL 2.0 datasets, which do not use weather stations within Bhutan for calibration. New precipitation surfaces better describe the heavy rainfall experienced in the southern foothills while retaining the effect of orography throughout the central valleys and ranges. The development of vapour pressure surfaces also allow for the calculation of ecologically important variables such as vapour pressure deficit, and may also be useful for solar radiation modelling in the region. The different datasets presented in this paper will facilitate ecological and agricultural research in Bhutan and provide high quality surfaces needed for future climate change scenarios.

Keywords: Bhutan, Himalayas, monsoon, climate, splines, interpolation, MODIS, temperature inversion

Introduction

The Himalayas comprise some of the most complex and extreme topography in the world, forming a natural barrier between the Tibetan plateau and the low-lying plains of the Indian subcontinent. The mountain range spans a distance of approximately 2,400 km from west to east, reaching peaks of over 8,500 m above sea level (asl) and crossing through Bhutan, India, Nepal, China and Pakistan. Uplift of the Himalayas and the Tibetan plateau over the past 50 million years has had large impacts upon the evolution of the Asian monsoon and intensified aridity in central Asia (Zhinsheng et al. 2001). Historically, the region has been of great interest to climatologists (Hill 1881; Flohn 1970; Barry 2008); however, few studies have focused specifically on the climatology of Bhutan.

Bhutan has an extremely diverse climate given its small size, which is due to the highly variable and complex topographic features that comprise the landscape. The climate is expected to change considerably over the coming decades (Singh et al. 2011) with mean annual temperature projected to increase by up to 3.5 °C and mean annual regional precipitation projected to increase between 80 mm and 180 mm by the 2050s (Tse-ring et al. 2010). High resolution climate datasets can facilitate ecological and agricultural research and land management decisions, as the spatial distribution and productivity of vegetation is heavily dependent upon climatic conditions (Austin & Van Niel 2011; Elith & Franklin 2013). Currently there is a paucity of spatial climate datasets calibrated using ground-based station observations for Bhutan which limits the ability to conduct robust assessments of climate and climate change on forests and agricultural ecosystems.

The latitudinal position in addition to the topographic extremes and complexity of the Himalayan region means that the climate has some unusual features. Temperature lapse rates show distinct trends that are associated with the seasonal reversal of the north Indian monsoon (Kattel et al. 2013; 2015; Dorji et al. 2016) and tend to be suppressed during the humid, cloudy, and wet summer months. Increased levels of atmospheric moisture and the forced ascent of air against the Himalayas result in cloud formation, precipitation and an associated release of latent heat (Ohata et al. 1981; Whiteman 2000; Barry 2008; Krishnamurti et al. 2013), particularly at higher elevations (Kattel et al. 2013). The cloudy conditions also cause more solar radiation to be reflected during the day, leading to cooler temperatures at lower elevations (Kattel et al. 2013). Kattel (et al. 2013) found residual errors were much larger for minimum temperatures than for maximum temperatures in Nepal and attribute this result to nocturnal temperature inversions. Temperature inversions typically develop under clear, calm conditions. At night time, thermal stratification of air in the lower troposphere (as a result of radiative cooling, subsidence, or convection of warm air over regions of cooler air) can cause a decoupling of the slope and valley atmospheres in mountainous terrain (Geiger 1965; Whiteman 2000; Barry 2008; Daly et al. 2009). As a consequence, cold air pools develop in basins and valley bottoms, and slopes become warmer due to convective processes. While this phenomenon is typically more pronounced in regions of complex topography, it may also manifest in comparatively flat terrain (Barry 2008; Kattel et al. 2013). Much weaker inversions are observed under windy conditions, or where cloud cover and water vapour decrease net longwave radiation losses (Iijima & Shinoda 2000; Whiteman et al. 2007; Zardi & Whiteman 2013). The spatial distribution of minimum temperature is therefore heavily dependent upon local terrain, and several studies have demonstrated that focal topographic metrics (Daly et al. 2007; Ashcroft & Gollan 2012) and

thermal remote sensing data (Stewart & Nitschke 2016) can be effective for improving minimum temperature interpolation performance.

Globally consistent climatologies such as WorldClim (Hijmans et al. 2005) and those developed by the Climatic Research Unit (CRU), University of East Anglia (New et al. 1999; New et al. 2002; Harris et al. 2014) can be used to extract climate data for most regions; however, they are somewhat limited for fine-scale ecological studies due to low spatial resolution and the variable density of suitable weather station data. The CRU suite of products are available at a spatial resolution of 18 km or 50 km, and are therefore limited in their ability to resolve the effects of fine scale topographic complexity on climate. Downscaling approaches (e.g. Wang et al. 2012) can be used to increase the spatial resolution of climate data; however, they typically rely on elevation dependencies and do not currently allow the incorporation of additional explanatory variables that can improve the quality of fine scale interpolations (Stewart & Nitschke 2016). WorldClim was developed at a much higher spatial resolution of approximately 1 km but does not provide data on variables such as humidity, sunshine duration and wind speed that are important ecologically. One of the key challenges in developing these globally representative surfaces is the availability of suitable station observations that are of sufficient density to capture regional scale climatological processes. Many regions of the world are underrepresented within these databases (CRU 2016; NOAA 2016; Hijmans et al. 2010), which can result in poor interpolation performance (Hijmans et al. 2005). The networks of weather stations typically used for these analyses do not include locations within Bhutan (CRU 2016; NOAA 2016; Hijmans et al. 2010). For example, the stations used for the WorldClim dataset (Figure 1; Hijmans et al. 2010) are sparse given the topographic complexity in this region, and many of the weather stations are no longer operational, particularly in India near the southern border

of Bhutan.

Until recently, the network of weather stations operating within Bhutan had not been used to develop spatially representative climate datasets for the region. Dorji (et al. 2016) used linear and polynomial regressions to describe the distribution of seasonal temperature and precipitation across Bhutan. The equations developed by Dorji (et al. 2016) are broadly representative of the region; however, they retain residual error when generating prediction surfaces and do not account for a spatially varying dependence upon elevation. Furthermore, extrapolating precipitation into the northern regions of Bhutan using polynomial regression and excluding the effects of orography are likely to lead to oversimplified predictions of rainfall.

The WorldClim and CRU CL 2.0 (New et al. 2002) datasets have been generated using trivariate thin plate smoothing splines (Wahba 1990) which are robust for climate interpolation (Hutchinson 1995; Hutchinson et al. 2009). Thin plate splines allow for a spatially varying dependence on elevation and minimise residual error at calibration locations; both of which are significant advantages over alternative methods such as linear regression. The thin plate spline algorithm is comprised of an affine component which is used to fit the global trend (as a function of spline variables) and a local non-affine component that adjusts the local non-linear surface. Trivariate splines are most commonly fit with full spline dependence upon latitude, longitude and elevation. Additional independent covariates can be incorporated by extension to a partial spline model, which includes a parametric regression component (Bates et al 1987).

147 The objective of this study was to develop improved temperature, precipitation and vapour
148 pressure datasets for Bhutan that address limitations of existing climate surfaces available for
149 the region. This was done by using the local weather station network in conjunction with
150 spline-based interpolation methods. The relative performance improvements that can be
151 achieved by including thermal remote sensing data and local topographic metrics as partial
152 spline dependencies when interpolating temperature variables were also assessed. These
153 variables have recently demonstrated an improvement in temperature interpolation
154 performance in topographically complex landscapes in southeast Australia (Stewart &
155 Nitschke 2016). The climate surfaces developed in this study were compared against the
156 globally representative WorldClim (Hijmans et al. 2005) and CRU CL 2.0 (New et al. 2002)
157 datasets in order to highlight the importance of spatial resolution and observation density
158 when developing interpolated climate surfaces.

159

160 **Method**

161 ***Study Site***

162 Bhutan is a land-locked country located on the southern slopes of the eastern Himalayas,
163 sharing borders with China to the north and India to the east, west and south. The largely
164 mountainous country is 38,394 km^2 in area and ranges from approximately 100 m asl in the
165 south to 7,500 m asl in the far north (Figure 2). The extreme range in elevation leads to
166 highly variable climatic conditions within a distance spanning only 170 km in latitude (Norbu
167 et al. 2003). Like many regions of Asia the climate of Bhutan is monsoonal. South-westerly
168 winds bring moist air from the Bay of Bengal to Bhutan during the summer phase of the
169 north Indian monsoon (Krishnamurti et al. 2013; Tamang 2014). The country has three
170 distinct climatic zones; alpine, temperate and subtropical (NSB 2015). The climate is humid
171 and subtropical in the southern plains and foothills (100 – 2,000 m asl), with heavy rainfall

occurring during the summer monsoon. The inner Himalayan valleys of the central regions have a temperate climate (2,000 – 4,000 m asl); however, they often receive less rainfall than the surrounding slopes and ridges as cloud cover and precipitation are suppressed by strong up-valley and up-slope winds (Barry 2008; Whiteman 2000). The high Himalayas to the north experience a cold alpine climate (4,000 m asl and above) and a permanent snow line can be found above 4,800 m asl (Tamang 2014). In winter, the snow line across the eastern Himalayas can descend to around 3,000 m asl (Mani 1981).

The estimated population of Bhutan is 784,000 (as of 2016), and approximately 56% of people are employed in the agricultural sector (NSB 2015; UN Data 2016). Over 70% of the country is under forest cover (Figure 3; LCMP 2011; NASA LP DAAC 2016). Bhutan hosts a diverse range of vegetation and forest types (Ohsawa 1987; LCMP 2011; NBSAP 2014), owing to the complex topography and corresponding climatic variability. The subtropical climate zone is comprised of broadleaf, chir pine (*Pinus roxburghii*) and tropical lowland forest. Fir, mixed conifer, blue pine (*Pinus wallichiana*) and mixed broadleaf and conifer forest can be found in the temperate climate zone, and the alpine climate zone consists of meadows and scrubs.

Datasets

Daily maximum temperature, minimum temperature, precipitation and relative humidity records for 71 weather stations operating between January 1986 and December 2015 were obtained from the Department of Hydro-Met Services (DHMS), Ministry of Economic Affairs, Bhutan. Latitude, longitude and elevation at each station were extracted from site metadata also provided by the DHMS. The network of stations used throughout the analysis was distributed across elevations ranging from 180 m asl to 3,537 m asl (Figure 1). The record length at each station was on average 19.6 years long, with a minimum of 6.7 years

and maximum of 30 years of observations. Daily records were excluded where the maximum temperature was reported as lower than the minimum temperature (795 daily records), relative humidity was below 0 % or above 100 % (128 daily records), or the amount of precipitation was negative (7 daily records).

Estimates of daily vapour pressure, rather than observations of relative humidity, were used to ensure dependence upon elevation. Daily vapour pressure was derived from the saturation vapour pressure of the mean daily temperature and relative humidity (Abtew & Melesse 2013). The mean daily temperature was calculated as the average of the maximum and minimum temperature. The saturation vapour pressure, e_s , was calculated using a reparameterisation (Alduchov & Eskridge 1996) of the August-Roche-Magnus equation (Lawrence 2005);

$$e_s(T) = 6.1094 \times exp^{\frac{17.625 \times T}{243.04+T}} \quad (1)$$

The daily vapour pressure, e, was then derived from the saturation vapour pressure at the mean temperature and relative humidity (RH);

$$e = e_s(T_{mean}) \times RH \quad (2)$$

Provisional climate normals (hereafter referred to as climate normals), representing the mean monthly conditions between 1986 and 2015, were calculated for maximum temperature, minimum temperature, precipitation and vapour pressure at each station. Monthly values were computed using daily observations prior to the calculation of mean monthly values. Monthly precipitation was calculated as the sum of daily precipitation where observations were available for each day of the month. Monthly mean temperature and vapour pressure

were calculated as the mean of each daily observation where the following criteria were met; (1) no more than 10 missing days of data were allowed, and (2) no more than 4 consecutive days of missing data were allowed (WMO 2011). Calculating climate normals for any reference period may be biased due to short or incomplete records at different observation locations. A regression patching approach was tested to correct for any potential bias induced by short term records by regressing observations against neighbouring stations (Hopkinson et al. 2012; Stewart & Nitschke 2016); however, this method did not produce reliable results. Monthly climate normals were therefore calculated for each station where at least 10 years of observations were available for each month (Hijmans et al. 2005) to ensure interpolation was supported by a sufficient number of data points in different locations and at the highest elevations.

Potential biases in short term means were investigated using interpolation variance and by analysing ranked residuals throughout the cross validation procedure for each variable. Stations were identified as suspect where the calculated mean value was more than 3.6 standard deviations from the cross validated prediction. This approach identified one suspect station which was subsequently removed from all analysis due to close proximity with neighbouring stations and short record length (10 years for each month). The removal of additional short term records selected based on ranked residuals consistently led to decreased performance at neighbouring stations (including those with more than 20 years of data) and therefore they were retained throughout the analysis. Excluding the suspect station and those with less than 10 years of data resulted in a satisfactory spatial and temporal coverage, with the number of stations available for analysis reduced by between 6 and 11 % for any variable or month.

246 The digital elevation model (DEM) used throughout the analysis was obtained from the
247 CGIAR Consortium for Spatial Information (http://srtm.csi.cgiar.org). This was resampled to
248 7.5 arc seconds (approx. 225 m cell resolution at the equator) using the sink-filled 3 arc
249 second (approx. 90 m cell resolution) Shuttle Radar Topography Mission (SRTM) dataset
250 (Jarvis et al. 2008). One of the issues with interpolating precipitation across a fine resolution
251 DEM is that the predictions are heavily influenced by local topography, leading to
252 unrealistically large differences at very small spatial scales. As precipitation is not strongly
253 correlated with elevation at distances up to 5 km to 10 km (Hutchinson 1998; Sharples et al.
254 2005), the original DEM was smoothed using a Gaussian filter for calibrating and predicting
255 precipitation (Barnes 1964; Daly et al. 2007). The use of a focal filter to smooth elevation
256 allows for precipitation surfaces to be generated at high resolution without extreme short
257 range variability. The degree of smoothing is determined by the filter extent and standard
258 deviation of the Gaussian distribution. The smoothing filter was applied with a circular search
259 diameter of 35 cells (approx. 7.8 km) and a standard deviation of 10 cells using the System
260 for Automated Geoscientific Analysis (SAGA) software package (Conrad et al. 2015). The
261 required level of smoothing was determined by iteratively adjusting the standard deviation of
262 the filter (5 to 25) and cross validating precipitation climate normals (Appendix S1).
263 Performance was optimal at a standard deviation of 10 cells, although the differences
264 between each level of smoothing varied by less than 1.5% in RMSE. Geographic coordinates
265 were expressed in decimal degrees and elevation expressed in kilometres during all analyses
266 (Hutchinson 1995; Hutchinson 1998; Hutchinson 2009) to minimise error during cross
267 validation and surface generation.

268

269 The effects of topographic position on minimum temperature were assessed using a
270 topographic index of relative elevation, which has been shown to improve model

271 performance by representing the effect of overnight temperature inversions and cold air
272 pooling processes (Daly et al. 2007; Ashcroft & Gollan 2012; Stewart & Nitschke 2016).
273 This index was calculated as the square root of the difference between the elevation at each
274 target cell and focal minimum within an 8.76 km circular search diameter. The optimal focal
275 range for the topographic index was systematically assessed by iteratively adjusting the
276 search diameter (1.1 km to 90.2 km) and cross validating minimum temperature (Appendix
277 S2).
278
279 Thermal remote sensing data from collection 6 of the Moderate Resolution Imaging
280 Spectroradiometer (MODIS) MOD11A2 (Wan et al. 2015) Land Surface Temperature (LST)
281 product (approx. 1 km cell resolution) was used as an independent covariate for temperature
282 interpolation. The MOD11A2 MODIS product can be effective in improving temperature
283 interpolation (Hengl et al. 2012; Stewart & Nitschke 2016) as it provides an indirect estimate
284 of land surface temperature and is sensitive to land cover classification (Snyder et al. 1998;
285 Wan 2006). All 8-day composite scenes available between February 2000 and December
286 2015 were downloaded using the *MODIS* package (Mattiuzzi 2016) in R (R Core Team
287 2016). Scenes were rejected where visual inspection indicated clear spatial artefacts, or the
288 number of cells with invalid LSTs was greater than 50% across Bhutan. This threshold was
289 set to ensure enough scenes were retained during the summer monsoon, when there is a very
290 high level of cloud cover. Each image was then transformed into z-scores, grouped by month
291 and averaged for each cell location. Outliers falling outside of the 95% confidence interval
292 were excluded when calculating the final mean value at each cell location (Stewart &
293 Nitschke 2016). Standardised monthly MODIS surfaces were calculated separately for day
294 scenes and night scenes to be used as predictors for interpolation of maximum temperature
295 and minimum temperature, respectively. Due to the extremely cloudy conditions and spatial

296 artefacts noted for several months during visual inspection of the LSTs, clear sky masks from
297 the MOD11A2 product were also used to support the analysis. Daily clear sky images were
298 extracted by converting 8-bit integers in the 8-day composite clear sky data to binary vectors.
299 The mean fraction of clear sky during the day and night was then calculated for each pixel,
300 and as a regional average, for each month.

301

302 ***Data Analysis***

303 Monthly maximum temperature, minimum temperature, precipitation and vapour pressure
304 climate normals for the 1986-2015 reference period were interpolated using trivariate splines
305 (Wahba 1990; Hutchinson 1995) in ANUSPLIN 4.4 (Hutchinson & Xu 2011). The spline
306 smoothing parameter was estimated using generalised cross validation (GCV; Craven &
307 Wahba 1979). For each variable, full spline dependence upon latitude, longitude and
308 elevation was assessed. Additional partial dependencies (Bates et al. 1987) were also assessed
309 for both maximum temperature (standardised MODIS day time LST) and minimum
310 temperature (standardised MODIS night time LST, topographic index). The square root of
311 vapour pressure (McKenney et al. 2004) and precipitation (Hutchinson 1995; Hutchinson
312 1998; Hutchinson 2009) climate normals were used for interpolation and the final predictions
313 were subsequently converted back to units of hectopascals (hPa) and millimetres.
314 ANUSPLIN internally corrects for the small amount of bias that arises as a result of these
315 transformations (Hutchinson & Xu 2011). As site elevations extracted from the smoothed
316 precipitation DEM are a function of the surrounding landscape they may differ from values
317 present in the site metadata (RMSE = 323 m). Precipitation was therefore cross validated
318 using both the actual and smoothed elevation values to ensure the smoothed interpolation
319 would produce reliable results.

320

Cross validation was performed by iteratively leaving out one observation and refitting the model until independent predictions were made for all locations. The coefficient of determination (r^2), mean absolute error (MAE), root mean square error (RMSE), ratio of the RMSE to the standard deviation of the observations (RSR; Moriasi et al. 2007) and mean error (BIAS) were used to assess model performance. Following cross validation, monthly climate normal surfaces were generated using all available stations for each model.

Residual analyses were performed to investigate the differences in model predictions when using alternative variables for interpolation, and also to compare the surfaces generated in this study against globally representative climate datasets. In order to detect differences in the spatial distribution of model predictions for temperature, residual values were calculated for each partial trivariate spline model by subtracting the trivariate spline with full dependence upon latitude, longitude and elevation. Empirical cumulative distribution plots were used to investigate the spread of mean annual maximum and minimum temperature residuals. November was selected to illustrate the spatial distribution of minimum temperature residuals.

Mean annual temperature and annual precipitation were extracted from the WorldClim (Hijmans et al. 2005) and the CRU CL 2.0 (New et al. 2002) datasets and compared against the new surfaces generated using the local weather station network. Residuals were calculated by subtracting the WorldClim and CRU surfaces from the gridded datasets generated in this study. Thermal remote sensing data is sensitive to land use type (Snyder et al. 1998; Wan 2006) and therefore partial spline models for temperature using standardised MODIS LST values were not assessed against the WorldClim or CRU datasets to ensure an appropriate comparison.

Results

Cross validated statistics for maximum temperature, minimum temperature, vapour pressure and precipitation climate normals are summarised in Table 1. All partial spline models for temperature variables provided a performance improvement over the full trivariate spline. Pooled statistics for maximum temperature demonstrate a 7.9 % improvement in RMSE over the full trivariate spline when using standardised day time MODIS LST values as an independent covariate. Pooled statistics for minimum temperature demonstrate an improvement of between 10.4 % and 12.3 % in RMSE when using standardised night time MODIS LST values, the topographic index, or their combination, as independent covariates. The use of smoothed DEM values rather than site elevations provided an 8.8% reduction in RMSE for precipitation. All variables achieved an RSR of 0.3 or less, indicating good model performance. Mean error (BIAS) was negligible for temperature and vapour pressure; however, there was a small negative bias for smoothed precipitation (-5.01 mm) which equated to -0.03 % as a proportion of the mean observed value.

The cross validated monthly RMSE for all variables and models summarised in Table 1 are illustrated in Figure 4. The partial trivariate spline for maximum temperature (3DS-M) was effective throughout the year and demonstrated the largest improvement between January and October (4.8% to 16.0% reduction in RMSE) when compared against the full trivariate spline (3DS). Partial spline models for minimum temperature (3DS-T, 3DS-M and 3DS-TM) were most effective in improving performance during the cooler months between October and April; however, they also provided a small improvement in May. Minimum temperature typically performed best during this period when including partial dependence upon both the standardised MODIS values and the topographic index (3DS-TM; 10.4% to 23.4% reduction

371 in RMSE when compared against 3DS). The RMSE of monthly precipitation climate normals
372 cross validated using the full trivariate spline (3DS) was highest during the wettest months
373 between May and September (RMSE between 55.8 mm and 120.7 mm). The ratio of the
374 RMSE to the mean was relatively stable across this period (29.3% to 37.1%), suggesting that
375 the high RMSE values are likely due to increased precipitation rather than reduced model
376 performance.

377

378 Daily MODIS acquisitions show that the fraction of clear sky over Bhutan is lowest during
379 the day between May and September (Figure 5). The regional mean vapour pressure is also
380 highest during these months. With the exception of May, partial spline models were
381 ineffective at improving minimum temperature interpolation performance throughout this
382 period when compared against the trivariate spline with full dependence upon latitude,
383 longitude and elevation. The clear sky fraction was on average lower during the night
384 between October and April.

385

386 The distribution of mean annual maximum and minimum temperature residuals, calculated by
387 subtracting the full trivariate spline (3DS) from each partial trivariate spline variant (3DS-T,
388 3DS-M and 3DS-TM), are presented in Figure 6. Mean annual maximum temperature
389 residuals (3DS-M) range from -4.2 °C to 4.8 °C and are cooler than the full trivariate spline
390 across 81.2 % of the region. Mean annual minimum temperature residuals (Figure 6)
391 demonstrate congruence between the partial trivariate spline models and are warmer across
392 68.2 % of cells for 3DS-T (-2.2 °C to 1.9 °C), 71.9% of cells for 3DS-M (-2.3 °C and 3.0 °C),
393 and 73.1% of cells for 3DS-TM (-2.1 °C and 2.6 °C).

394

Minimum temperature residuals in November (Figure 7) show a similar spatial distribution for all models, with a warming of slopes and cooling of areas with low relative elevation. Minimum temperature interpolation using standardised MODIS LST values show a much broader range of values in comparison to variants using only topographic metrics. Residuals were up to 1.8 °C cooler and 1.3 °C warmer for 3DS-TM in comparison to the maximum range predicted by 3DS-T.

The spatial distribution of mean annual temperature and annual precipitation interpolated using the local weather station network (maximum temperature 3DS; minimum temperature 3DS-T; precipitation 3DS) show large deviations from the WorldClim and CRU CL 2.0 datasets (Figure 8). The regional mean annual temperature for locally calibrated interpolations was 0.75 °C warmer than the WorldClim dataset, and 1.81 °C warmer than the CRU dataset. This result was most pronounced across the western regions of Bhutan in the WorldClim dataset. For mean annual temperature, the residuals between the new surfaces and the WorldClim values varied by as much as 5.9 °C and the residuals between the new surfaces and the CRU values varied by up to 12.9 °C. The 3DS model predicts the greatest amount of precipitation across the southern foothills of Bhutan; however, unlike the WorldClim and CRU datasets, these high rainfall regions do not extend into the central valleys. Precipitation residuals show deviations of up to 3,364 mm in the WorldClim dataset, and up to 2,845 mm in the CRU dataset when compared against locally calibrated interpolation. Precipitation typically decreases with elevation across Bhutan in the WorldClim and CRU datasets. The 3DS model exhibits an increase in precipitation with elevation across the central valleys and a decrease in overall precipitation towards the far north of Bhutan.

Discussion

The results of this study demonstrate the advantages of incorporating MODIS LST data and local topographic indices as additional partial dependencies when interpolating temperature variables across topographically complex landscapes, such as those in Bhutan. Stewart and Nitschke (2016) found similar outcomes for the effectiveness of these variables in southeast Australia, despite large differences in topographic and climatic conditions. They found that MODIS LST values improved maximum temperature interpolation performance the most during the warm summer months. In Bhutan, the largest improvements in maximum temperature interpolation performance were also achieved during the warmest months when using standardised MODIS LST values as an independent covariate. This performance improvement was maintained throughout the summer monsoon, despite heavy day time cloud cover which reduced the amount of data available to construct standardised surfaces. The MOD11A2 product is sensitive to land cover classification, and therefore the seasonal performance differences may be due to the indirect detection of spatially aggregated microclimatic conditions responding to higher temperatures, particularly during the summer months.

Both the MODIS LST values and local topographic metrics were effective at improving minimum temperature interpolation performance during the dry months between October and May; however, neither provided a performance improvement between June and September. This congruence suggests that MODIS LST data may be particularly effective at detecting temperature inversion signals in the long term climate record, and also indicates that the effectiveness of these variables may be considerably reduced during cloudy, wet and humid conditions that are characteristic of the summer monsoon in Bhutan. The extensive cloud cover observed during these months did not have a negative impact on maximum temperature

445 performance when using MODIS LST values, and therefore the lack of performance
446 improvement for minimum temperatures was likely due to the absence of a detectable
447 inversion effect in the long term record, rather than as a result of poor data quality. The
448 release of latent heat and suppression of outgoing longwave radiation associated with
449 extensive cloud cover, heavy precipitation and high vapour pressure are likely to overcome
450 the influence of temperature inversions and local topography during the wet months of the
451 summer monsoon. These conditions are likely to suppress temperature inversion regimes due
452 to their influence upon the surface energy balance (Iijima & Shinoda 2000; Whiteman et al.
453 2007; Barry 2008; Zardi & Whiteman 2013). The nocturnal release of latent heat has also
454 been associated with the persistence of up-slope and up-valley winds in the eastern
455 Himalayas (Ohata et al. 1981; Barry 2008), which may further suppress thermal stratification
456 of air near the surface and the development of cold air flows and pools. Both variables were,
457 however, effective at improving minimum temperature interpolation performance between
458 October and May. When included separately as partial dependencies, each variable led to a
459 warming of slopes and a cooling of valley bottoms when compared against the trivariate
460 spline with full dependence upon latitude, longitude and elevation. This result is consistent
461 with the current understanding of nocturnal temperature distributions in mountainous terrain
462 (Geiger 1965; Whiteman 2000; Barry 2008).

463

464 Horizontal scaling of the topographic index resulted in an optimal search diameter of
465 approximately 8.8 km, which is 5 times greater than the optimal diameter identified for
466 southeast Australia (Stewart & Nitschke 2016). Furthermore, using both MODIS LST data
467 and the topographic index provided an additive improvement in minimum temperature
468 performance in southeast Australia that was not found for Bhutan. This is potentially due to
469 the scale of topographic variation in Bhutan (southeast Australia is comparatively much

flatter with small peak-to-peak distances in the alpine regions) and the ability of the MODIS LST data to detect temperature inversions at appropriate scales. These results suggest that a spatially varying dependence upon the topographic index, calculated with short search diameters, in conjunction with MODIS LST data may allow for spatial interpolation of current minimum temperatures at much greater spatial extents. This may prove useful for spatial predictions of current climate; however, thermal remote sensing data is sensitive to land cover and therefore should not be used for projecting climate change scenarios.

When utilising the local weather station network in Bhutan, new precipitation surfaces were able to characterise the heavy rainfall experienced in the southern foothills while retaining the effect of orography on precipitation throughout the central valleys and ranges. Precipitation is suppressed across the interior of these valleys and ranges by strong up-valley and up-slope winds (Whiteman 2000), which can lead to an underestimation of rainfall throughout the central regions of Bhutan (Norbu et al. 2003). Historical rainfall data and the distribution of vegetation suggests that the slopes and ridges throughout these regions are wetter than the inner valleys (Ohsawa 1987; Norbu et al. 2003), which is reflected in the spatial distribution of precipitation predicted in this study. The precipitation surfaces presented should be interpreted with a degree of caution, as much of the precipitation in the higher elevation regions of Bhutan falls as snow and elevations above 3,537 m asl are not represented by the local weather station network. Furthermore, precipitation is highly variable in the southern foothills of Bhutan and the representativeness of mean conditions is therefore dependent upon the available data series length.

The importance of spatial resolution and observation density is apparent when comparing the datasets developed as part of this study against globally consistent climate datasets such as

WorldClim and CRU CL 2.0. Analyses of the CRU CL 2.0 residuals show that the within-cell mean annual temperature variability can be as high as 20 °C for coarse resolution products in Bhutan. While downscaling approaches are an option, they cannot incorporate the effects of mesoscale processes such as temperature inversions. The temperature bias that is evident in the WorldClim residuals across western Bhutan, where temperatures are often at least 2.5 °C cooler than predicted in the present study, indicate the importance of observation density and placement. It is unlikely that this region has experienced such an increase in mean annual temperature given that the datasets compared are centred on reference periods that differ by only 25 years. The analyses of precipitation residuals show extreme deviations between the present study and both the WorldClim and CRU CL 2.0 datasets. These results support conclusions by Hijmans (et al. 2005) that station density is perhaps the most important factor for inferring the quality of interpolated climate datasets. Station observations that qualify for inclusion in global databases may be limited in many cases due to data and weather station availability, insufficient length of records, or lack of quality control processes. When globally representative surfaces such as WorldClim are used for regional studies, an evaluation of point density and topographic variability is recommended to evaluate whether or not these surfaces are likely to capture climatological processes at appropriate scales. Acquisition and interpolation of regional weather station data may be justified, and in some cases required, where the point density is too low.

The temperature and vapour pressure surfaces generated as part of this study allow for the spatial estimation of vapour pressure deficit and relative humidity. These variables can be critical for modelling vegetation distributions, as they characterise the atmospheric demand for moisture. While outside the scope of the present study, vapour pressure surfaces may also be used for atmospheric attenuation when modelling potential incoming solar radiation (e.g.

Böhner & Antoni 2009; Conrad et al. 2015). Vapour pressure precludes the need for estimates of lumped atmospheric transmittance, and allows for the effects of elevation to be incorporated into solar radiation predictions. Solar radiation modelling in Bhutan is, however, likely to be complicated by heavy cloud cover, particularly during the summer monsoon. Observations of sunlight hours are available at a small number of stations within the local weather station network in Bhutan, which may facilitate the production of high quality solar radiation surfaces in the future.

Conclusion

The datasets presented in this paper provide a new resource for ecological and agricultural research in Bhutan. Alternative versions of temperature variables were generated to provide the highest quality surfaces (MODIS LST variants) and to maximise compatibility with climate change projections (topographic index). These temperature datasets are calibrated specifically for Bhutan using the local weather station network, are sensitive to the climatic conditions present during the summer monsoon, and incorporate inversion signals that cannot be detected using existing methodologies for statistical downscaling. Both the topographic index and the standardised night time MODIS LST values show evidence that they can detect the effects of temperature inversions on minimum temperature climate normals. These particular covariates are rarely used to improve temperature interpolation, and therefore their application is novel for the region. Precipitation surfaces characterise the heavy precipitation observed in the southern foothills, while retaining the effects of orography throughout the central regions of Bhutan. These effects are absent from global climate surfaces as they do not include weather station observations from within Bhutan. Incorporating the effect of orography on precipitation using trivariate spline interpolation provides a large improvement over polynomial regression techniques that have previously been applied in Bhutan. Globally

545 representative humidity data is very coarse in resolution. The inclusion of vapour pressure
546 surfaces allows for the calculation of humidity metrics and vapour pressure deficit, which
547 will further facilitate ecological modelling and assist in decision making for climate change
548 adaptation throughout Bhutan.

549

550 **Acknowledgements**

551 We would like to thank the Department of Hydro-Met Services (DHMS), Ministry of
552 Economic Affairs, Bhutan, for providing weather station data which made this research
553 possible. The research was supported by the Melbourne Research Scholarship (University of
554 Melbourne) with additional funding provided by the State of Victoria Department of
555 Environment, Land, Water and Planning (DELWP) though the Integrated Forest Ecosystem
556 Research (iFER) program.

557

558 **References**

559 Abtew W, Melesse A. 2013. Vapour pressure calculation methods. In: Evaporation and
560 evapotranspiration: measurements and estimations. Springer: Netherlands. doi:
561 10.1007/978-94-007-4737-1.

562 Alduchov OA, Eskridge RE. 1996. Improved Magnus form approximation of saturation
563 vapour pressure. *Journal of Applied Meteorology* **34(4):** 601-609. doi: 10.1175/1520-
564 0450(1996)035<0601:IMFAOS>2.0.CO;2.

565 Ashcroft MB, Gollan JR. 2012. Fine-resolution (25 m) topoclimatic grids of near-surface (5
566 cm) extreme temperatures and humidities across various habitats in a large (200 / x 300
567 km) and diverse region. *International Journal of Climatology* **32(14):** 2134-2148.

doi:10.1002/joc.2428.

Austin MP, Van Niel KP. 2011. Improving species distribution models for climate change studies: variable selection and scale. *Journal of Biogeography* **38(1):** 1-8. doi: 10.1111/j.1365-2699.2010.02416.x.

Barnes SL. 1964. A technique for maximizing details in numerical weather map analysis. *Journal of Applied Meteorology* **3(4):** 396-409. doi: 10.1175/1520-0450(1964)003<0396:ATFMDI>2.0.CO;2.

Barry RG. 2008. Mountain weather and climate. Cambridge University Press: Cambridge, United Kingdom. doi: 10.1017/CBO9780511754753.

Bates DM, Lindstrom MJ, Wahba G, Yandell BS. 1987. GCVPACK–routines for generalized cross validation. *Communications in Statistics-Simulation and Computation* **16(1):** 263-297.

Bonan GB, Levis S, Kergoat L, Oleson, KW. 2002. Landscapes as patches of plant functional types: an integrating concept for climate and ecosystem models. *Global Biogeochemical Cycles* **16(2)**. doi: 10.1029/2000GB001360

Böhner J, Antoni O. 2009. Chapter 8: Land-surface parameters specific to topo-climatology. *Developments in Soil Science* **33:** 195-226. doi:10.1016/S0166-2481(08)00008-1.

Climatic Research Unit (CRU). 2016. *Land Stations used by the Climatic Research Unit within CRUTEM3*. University of East Anglia: Norwich, United Kingdom. https://crudata.uea.ac.uk/cru/data/landstations/. Accessed 1 August 2016.

Conrad O, Bechel B, Bock M, Dietrich H, Fischer E, Gerlitz L, Wehberg J, Wichmann V, Böhner J. 2015. System for automated geoscientific analyses (SAGA) v. 2.1.4. *Geoscientific Model Development* **8(7):** 1991-2007. doi: 10.5194/gmd-8-1991-2015.

Craven P, Wahba G. 1979. Smoothing noisy data with spline functions: Estimating the

592 correct degree of smoothing by the method of generalized cross-validation. *Numerische*
593 *Mathematik* **31:** 377-403.

594 Daly C, Smith JW, Smith JI, McKane RB. 2007. High-resolution spatial modelling of daily
595 weather elements for a catchment in the Oregon Cascade Mountains, United States.
596 *Journal of Applied Meteorology and Climatology* **46(10):** 1565–1586. doi:
597 10.1175/JAM2548.1.

598 Daly C, Conklin DR, Unsworth MH. 2009. Local atmospheric decoupling in complex
599 topography alters climate change impacts. *International Journal of Climatology* **30(12):**
600 1857-1864. doi: 10.1002/joc.2007.

601 Dorji U, Olesen JE, Bøcher PK, Seidenkrantz MS. 2016. Spatial variation of temperature and
602 precipitation in Bhutan and links to vegetation and land cover. *Mountain Research and*
603 *Development* **36(1)**: 66-79. doi: http://www.bioone.org/doi/10.1659/MRD-JOURNAL-
604 D-15-00020.1.

605 Elith J, Franklin J. 2013. Species Distribution Modeling. *Encyclopedia of Biodiversity* **6:**
606 692–705. doi:10.1016/B978-0-12-384719-5.00318-X.

607 Flohn H. 1970. Beiträge zur meteorologie des Himalaya. *Khumbu Himal.* **7(2)**: 25-45.

608 Friedl MA, Sulla-Menashe D, Tan B, Schneider A, Ramankutty N, Sibley A, Huang X. 2010.
609 MODIS collection 5 global land cover: algorithm refinements and characterization of
610 new datasets. *Remote Sensing of Environment* **114(1)**: 168-182. doi:
611 10.1016/j.rse.2009.08.016.

612 Geiger R. 1965. Climate near the ground. Harvard University Press: Cambridge,
613 Massachusetts, United States.

614 Harris I, Jones PD, Osborn TJ, Lister DH. 2014. Updated high-resolution grids of monthly
615 climatic observations – the CRU TS3.10 dataset. *International Journal of Climatology*

34(3): 623-642. doi: 10.1002/joc.3711.

Hengl T, Heuvelink GBM, Per ec Tadi M, Pebesma EJ. 2012. Spatio-temporal prediction of daily temperatures using time-series of MODIS LST images. *Theoretical and Applied Climatology* **107:** 265-277. doi:10.1007/s00704-011-0464-2.

Hijmans RJ, Cameron SE, Parra JL, Jones PG, Jarvis A. 2005. Very high resolution interpolated climate surfaces for global land areas. *International Journal of Climatology* **25(15):** 1965-1978. doi:10.1002/joc.1276.

Hijmans RJ, Cameron SE, Parra JL, Jones PG, Jarvis A. 2010. *WorldClim: global weather stations*. ESRI. https://www.arcgis.com/home/item.html?id=7644c6e78c1644b4bde2edfc44787520/. Accessed 1 August, 2016.

Hill SA. 1881. The meteorology of the north-west Himalaya. *Memoirs of the India Meteorological Department*. **1**: 377-429.

Hopkinson RF, Hutchinson MF, McKenney DW, Milewska EJ, Padadopol P. 2012. Optimizing input data for gridding climate normals for Canada. *Journal of Applied Meteorology and Climatology* **51**(8): 1508-1518. doi:10.1175/JAMC-D-12-018.1.

Hutchinson MF. 1995. Interpolating mean rainfall using thin plate smoothing splines. *International journal of geographical information systems* **9(4):** 385-403. doi:10.1080/02693799508902045.

Hutchinson, MF. 1998. Interpolation of rainfall data with thin-plate smoothing splines II: Analysis of topographic dependence. *Journal of Geographic Information and Decision Analysis* **2(2)**: 152-167.

Hutchinson MF, McKenney DW, Lawrence K, Pedlar JH, Hopkinson RF, Milewska E, Papadopol P. 2009. Development and testing of Canada-wide interpolated spatial

640 models of daily minimum-maximum temperature and precipitation for 1961 – 2003.
641 *Journal of Applied Meteorology and Climatology* **48(4):** 725-741.
642 doi:10.1175/2008JAMC1979.1.

643 Hutchinson MF, Xu T. 2013. ANUSPLIN Version 4.4 User Guide.

644 Iijima Y, Shinoda M. 2000. Seasonal changes in the cold-air pool formation in a subalpine
645 hollow, central Japan. *International Journal of Climatology* **20(12):** 1471-1483. doi:
646 10.1002/1097-0088(200010)20:12<1471::AID-JOC554>3.0.CO;2-6.

647 Jarvis A, Reuter HI, Nelson A, Guevara E. 2008. Hole-filled seamless SRTM data V4.
648 International Centre for Tropical Agriculture (CIAT). http://srtm.csi.cgiar.org.

649 Kattel DB, Yao T, Yang K, Tian L, Yang G, Joswiak D. 2013. Temperature lapse rate in
650 complex mountain terrain on the southern slope of the central Himalayas. *Theoretical*
651 *and Applied Climatology* **113:** 671-682. doi: 10.1007/s00704-012-0816-6.

652 Kattel DB, Yao T, Yang W, Gao Y, Tian L. 2015. Comparison of temperature lapse rates
653 from the northern to the southern slopes of the Himalayas. *International Journal of*
654 *Climatology* **35(15):** 4431-4443. Doi: 10.1002/joc.4297.

655 Krishnamurti TN, Stefanova , Misra V. 2013. Tropical meteorology. Springer: New York,
656 United States. doi: 10.1007/978-1-4614-7409-8.

657 Land Cover Mapping Project (LCMP). 2011. *Technical report: Bhutan land cover*
658 *assessment 2010 (LCMP-2010).* National Soil Services Centre (NSSC) and Policy and
659 Planning Division (PPD). Ministry of Agriculture and Forests. Royal Government of
660 Bhutan.

661 Lawrence M. 2005. The relationship between relative humidity and the dewpoint temperature
662 in moist air: a simple conversion and applications. *Bulletin of the American*
663 *Meteorological Society* **86(2):** 225-233. doi: 10.1175/BAMS-86-2-225.

Mani A. 1981. The climate of the Himalaya. In: Lall JS, Moddie AD (eds). The Himalaya: aspects of changes. Oxford University Press: New Delhi, India.

Mattiuzzi M. 2016. *MODIS: MODIS Acquisition and Processing*. R package version 0.10-34/r510. https://R-Forge.R-project.org/projects/modis/. Accessed 1 August, 2016.

McKenney DW, Hutchinson MF, Papadopol P, Price DT. 2004. Evaluation of alternative spatial models of vapour pressure in Canada. Proceedings: 26th Conference on Agricultural and Forest Meteorology. August 23-27. Vancouver, British Columbia. Natural Resources Canada, Great Lakes Forestry Centre.

Moriasi DN, Arnold JG, Van Liew MW, Bingner RL, Harmel RD, Veith TL. 2007. Model evaluation guidelines for systematic quantification of accuracy in watershed simulations. *Transactions of the ASABE* **50(3):** 885-900. doi:10.13031/2013.23153.

NASA LP DAAC. 2016. MCD12Q1 Land Cover Type Yearly L3 Global 500 m SIN Grid .V051. NASA EOSDIS Land Processes DAAC, USGS Earth Resources Observation and Science (EROS) Center: Sioux Falls, South Dakota (https://lpdaac.usgs.gov).

National Biodiversity Strategies and Action Plan of Bhutan (NBSAP). 2014. National Biodiversity Centre. Ministry of Agriculture and Forests. Royal Government of Bhutan.

National Oceanic and Atmospheric Administration (NOAA). 2016. Global historical climate network (GHCN). National Centres for Environmental Information: United States.

National Statistics Bureau (NSB). 2015. Statistical yearbook of Bhutan. National Statistics Bureau. Royal Government of Bhutan. http://www.nsb.gov.bt/.

New M, Hulme M, Jones, P. 1999. Representing twentieth-century space-time climate variability. Part I: Development of a 1961-90 mean monthly terrestrial climatology. *Journal of Climate* **12(3):** 829-856. doi:10.1175/1520-0442(1999)012<0829:RTCSTC>2.0.CO;2.

New M, Lister D, Hulme M, Makin I. 2002. A high-resolution data set of surface climate over global land areas. *Climate Research* **21(1):** 1–25. doi:10.3354/cr021001.

Norbu C, Baillie I, Dorji T, Dorj T, Tamang HB, Tshering K, Hutcheon A. 2003. A provisional physiographic zonation of Bhutan. *Journal of Bhutan Studies* **8:** 54-87.

Ohata T, Higuchi K, Ikegami K. 1981. Mountain-valley wind system in the Khumbu Himal, east Nepal. *Journal of the Meteorological Society of Japan*: 59(5): 753-762.

Ohsawa M. 1987. Vegetation zones in the Bhutan Himalaya. In: Ohsawa M (ed). Life zone ecology of the Bhutan Himalaya. Chiba University: Tokyo, Japan.

R Core Team, 2016. R: A language and environment for statistical computing. R Foundation for Statistical Computing: Vienna, http://www.R-project.org/.

Sharples JJ, Hutchinson MF, Jellet DR. 2005. On the horizontal scale of elevation dependence of Australian monthly precipitation. *Journal of Applied Meteorology* **44(12):** 1850-1865. doi: 10.1175/JAM2289.1.

Singh SP, Bassignana-Khadka I, Karky BS, Sharma E. 2011. *Climate change in the Hindu Kush-Himalayas: the state of current knowledge*. International Centre for Integrated Mountain Development (ICIMOD): Kathmandu, Nepal.

Snyder WC, Wan Z, Zhang Y, Feng Y-Z. 1998. Classification-based emissivity for land surface temperature measurement from space. International Journal of Remote Sensing 19(14): 2753-2774.

Stewart SB, Nitschke CR. 2016. Improving temperature interpolation using MODIS LST and local topography: a comparison of methods in south east Australia. *International Journal of Climatology*. doi: 10.1002/joc.4902.

Tamang TB. 2014. *Bhutan country presentation*. Regional Workshop on Implementation of Weather and Climate-related Services in the Least Developed Countries (LDCs) in Asia:

712 9-11 September, Thimphu, Bhutan.

713 Tse-ring K, Sharma E, Chettri N, Shrestha A (eds). 2010. Climate change vulnerability of
714 mountain ecosystems in the eastern Himalayas. International Centre for Integrated
715 Mountain Development (ICIMOD): Kathmandu, Nepal.

716 UN Data. 2016. *Country profile: Bhutan*. United Nations Statistics Division: New York,
717 United States. http://data.un.org/. Accessed 20 August, 2016.

718 Wahba G. 1990. *Spline models for observational data*. SIAM: Society for Industrial and
719 Applied Mathematics: Philadelphia, United States.

720 Wan Z. 2006. Collection-5 MODIS land surface temperature products users' guide.
721 http://www.icess.ucsb.edu/modis/LstUsrGuide/usrguide.html.

722 Wan Z, Hook S, Hulley G. 2015. MOD11A2 MODIS/Terra Land Surface
723 Temperature/Emissivity 8-Day L3 Global 1km SIN Grid V006. NASA EOSDIS Land
724 Processes DAAC, USGS Earth Resources Observation and Science (EROS) Center:
725 Sioux Falls, South Dakota (https://lpdaac.usgs.gov). doi:
726 10.5067/MODIS/MOD11A2.006.

727 Wang T, Hamann A, Spittlehouse DL, Murdock TQ. 2012. ClimateWNA—high-resolution
728 spatial climate data for Western North America. *Journal of Applied Meteorology and*
729 *Climatology* **51(1):** 16-29. doi:10.1175/JAMC-D-11-043.1.

730 Whiteman DC. 2000. Mountain meteorology: fundamentals and applications. Oxford
731 University Press: United Kingdom. ISBN: 0195132718.

732 Whiteman DC, De Wekker SFJ, Haiden T. 2007. Effect of dewfall and frostfall on nightime
733 cooling in a small, closed basin. *Journal of Applied Meteorology* **46:** 3-13. doi:
734 10.1175/JAM2453.1.

735 World Meteorological Organization (WMO). 2011. Guide to Climatological Practices.

WMO-No. 100. World Meteorological Organization: Geneva, Switzerland.

Zardi D, Whiteman DC. 2013. Diurnal mountain wind systems. In: Chow FK, De Wekker SFJ, Snyder BJS (eds). Mountain weather research and forecasting. Springer: New York, United States. doi: 10.1007/978-94-007-4098-3.

Zhisheng A, Kutzbach JE, Prell WL, Porter, SC. 2001. Evolution of Asian monsoons and phased uplift of the Himalaya-Tibetan plateau since late Miocene times. *Nature* **411**: 62-66. doi: 10.1038/35075035.

The role of topography and the north Indian monsoon on mean monthly climate interpolation within the Himalayan Kingdom of Bhutan

Stewart, Stephen B[1,3], Choden, Kunzang[2], Fedrigo, Melissa[3,4], Roxburgh, Stephen H[3], Keenan, Rodney[2], Nitschke, Craig R[1].

1 School of Ecosystem and Forest Sciences, Faculty of Science, University of Melbourne, 500 Yarra Boulevard, Richmond, Victoria, 3121, Australia.

2 School of Ecosystem and Forest Sciences, Faculty of Science, University of Melbourne, Grattan Street, Parkville, Victoria, 3010, Australia.

3 CSIRO Land and Water, GPO Box 1700, Canberra, Australian Capital Territory, 2601, Australia.

4 Centre for Tropical Environmental and Sustainability Studies, James Cook University, PO Box 6811, Cairns, Queensland, 4870, Australia.

Corresponding author:

Stephen Stewart

500 Yarra Boulevard, Richmond, VIC, 3121, Australia

stephen.stewart85@gmail.com

+61 402 766 147

Abstract

Spatial climate datasets currently available for Bhutan are limited by weather station data availability, spatial resolution, or interpolation methodology. This paper presents new datasets for monthly maximum temperature, minimum temperature, precipitation and vapour pressure climate normals interpolated for the 1986-2015 reference period using trivariate smoothing splines. The inclusion of standardised day time Moderate Resolution Imaging Spectroradiometer (MODIS) land surface temperature (LST) values as partial spline dependencies reduced cross validated RMSE for maximum temperature by up to 16.0% and was most effective between March and September. Using both a topographic index of relative elevation and standardised night time MODIS LST values as partial spline dependencies reduced monthly mean minimum temperature RMSE by up to 23.4%. Neither variable was effective for minimum temperature interpolation between June and September. High humidity, extensive cloud cover and heavy precipitation occur during these months, which are likely to suppress the formation of temperature inversions that typically form under clear, calm conditions. These new temperature and precipitation surfaces show distinct differences from the WorldClim and CRU CL 2.0 datasets, which do not use weather stations within Bhutan for calibration. New precipitation surfaces better describe the heavy rainfall experienced in the southern foothills while retaining the effect of orography throughout the central valleys and ranges. The development of vapour pressure surfaces also allow for the calculation of ecologically important variables such as vapour pressure deficit, and may also be useful for solar radiation modelling in the region. The different datasets presented in this paper will facilitate ecological and agricultural research in Bhutan and provide high quality surfaces needed for future climate change scenarios.

Keywords: Bhutan, Himalayas, monsoon, climate, splines, interpolation, MODIS, temperature inversion

Introduction

The Himalayas comprise some of the most complex and extreme topography in the world, forming a natural barrier between the Tibetan plateau and the low-lying plains of the Indian subcontinent. The mountain range spans a distance of approximately 2,400 km from west to east, reaching peaks of over 8,500 m above sea level (asl) and crossing through Bhutan, India, Nepal, China and Pakistan. Uplift of the Himalayas and the Tibetan plateau over the past 50 million years has had large impacts upon the evolution of the Asian monsoon and intensified aridity in central Asia (Zhinsheng et al. 2001). Historically, the region has been of great interest to climatologists (Hill 1881; Flohn 1970; Barry 2008); however, few studies have focused specifically on the climatology of Bhutan.

Bhutan has an extremely diverse climate given its small size, which is due to the highly variable and complex topographic features that comprise the landscape. The climate is expected to change considerably over the coming decades (Singh et al. 2011) with mean annual temperature projected to increase by up to 3.5 °C and mean annual regional precipitation projected to increase between 80 mm and 180 mm by the 2050s (Tse-ring et al. 2010). High resolution climate datasets can facilitate ecological and agricultural research and land management decisions, as the spatial distribution and productivity of vegetation is heavily dependent upon climatic conditions (Austin & Van Niel 2011; Elith & Franklin 2013). Currently there is a paucity of spatial climate datasets calibrated using ground-based station observations for Bhutan which limits the ability to conduct robust assessments of climate and climate change on forests and agricultural ecosystems.

The latitudinal position in addition to the topographic extremes and complexity of the Himalayan region means that the climate has some unusual features. Temperature lapse rates show distinct trends that are associated with the seasonal reversal of the north Indian monsoon (Kattel et al. 2013; 2015; Dorji et al. 2016) and tend to be suppressed during the humid, cloudy, and wet summer months. Increased levels of atmospheric moisture and the forced ascent of air against the Himalayas result in cloud formation, precipitation and an associated release of latent heat (Ohata et al. 1981; Whiteman 2000; Barry 2008; Krishnamurti et al. 2013), particularly at higher elevations (Kattel et al. 2013). The cloudy conditions also cause more solar radiation to be reflected during the day, leading to cooler temperatures at lower elevations (Kattel et al. 2013). Kattel (et al. 2013) found residual errors were much larger for minimum temperatures than for maximum temperatures in Nepal and attribute this result to nocturnal temperature inversions. Temperature inversions typically develop under clear, calm conditions. At night time, thermal stratification of air in the lower troposphere (as a result of radiative cooling, subsidence, or convection of warm air over regions of cooler air) can cause a decoupling of the slope and valley atmospheres in mountainous terrain (Geiger 1965; Whiteman 2000; Barry 2008; Daly et al. 2009). As a consequence, cold air pools develop in basins and valley bottoms, and slopes become warmer due to convective processes. While this phenomenon is typically more pronounced in regions of complex topography, it may also manifest in comparatively flat terrain (Barry 2008; Kattel et al. 2013). Much weaker inversions are observed under windy conditions, or where cloud cover and water vapour decrease net longwave radiation losses (Iijima & Shinoda 2000; Whiteman et al. 2007; Zardi & Whiteman 2013). The spatial distribution of minimum temperature is therefore heavily dependent upon local terrain, and several studies have demonstrated that focal topographic metrics (Daly et al. 2007; Ashcroft & Gollan 2012) and

thermal remote sensing data (Stewart & Nitschke 2016) can be effective for improving minimum temperature interpolation performance.

Globally consistent climatologies such as WorldClim (Hijmans et al. 2005) and those developed by the Climatic Research Unit (CRU), University of East Anglia (New et al. 1999; New et al. 2002; Harris et al. 2014) can be used to extract climate data for most regions; however, they are somewhat limited for fine-scale ecological studies due to low spatial resolution and the variable density of suitable weather station data. The CRU suite of products are available at a spatial resolution of 18 km or 50 km, and are therefore limited in their ability to resolve the effects of fine scale topographic complexity on climate. Downscaling approaches (e.g. Wang et al. 2012) can be used to increase the spatial resolution of climate data; however, they typically rely on elevation dependencies and do not currently allow the incorporation of additional explanatory variables that can improve the quality of fine scale interpolations (Stewart & Nitschke 2016). WorldClim was developed at a much higher spatial resolution of approximately 1 km but does not provide data on variables such as humidity, sunshine duration and wind speed that are important ecologically. One of the key challenges in developing these globally representative surfaces is the availability of suitable station observations that are of sufficient density to capture regional scale climatological processes. Many regions of the world are underrepresented within these databases (CRU 2016; NOAA 2016; Hijmans et al. 2010), which can result in poor interpolation performance (Hijmans et al. 2005). The networks of weather stations typically used for these analyses do not include locations within Bhutan (CRU 2016; NOAA 2016; Hijmans et al. 2010). For example, the stations used for the WorldClim dataset (Figure 1; Hijmans et al. 2010) are sparse given the topographic complexity in this region, and many of the weather stations are no longer operational, particularly in India near the southern border

of Bhutan.

Until recently, the network of weather stations operating within Bhutan had not been used to develop spatially representative climate datasets for the region. Dorji (et al. 2016) used linear and polynomial regressions to describe the distribution of seasonal temperature and precipitation across Bhutan. The equations developed by Dorji (et al. 2016) are broadly representative of the region; however, they retain residual error when generating prediction surfaces and do not account for a spatially varying dependence upon elevation. Furthermore, extrapolating precipitation into the northern regions of Bhutan using polynomial regression and excluding the effects of orography are likely to lead to oversimplified predictions of rainfall.

The WorldClim and CRU CL 2.0 (New et al. 2002) datasets have been generated using trivariate thin plate smoothing splines (Wahba 1990) which are robust for climate interpolation (Hutchinson 1995; Hutchinson et al. 2009). Thin plate splines allow for a spatially varying dependence on elevation and minimise residual error at calibration locations; both of which are significant advantages over alternative methods such as linear regression. The thin plate spline algorithm is comprised of an affine component which is used to fit the global trend (as a function of spline variables) and a local non-affine component that adjusts the local non-linear surface. Trivariate splines are most commonly fit with full spline dependence upon latitude, longitude and elevation. Additional independent covariates can be incorporated by extension to a partial spline model, which includes a parametric regression component (Bates et al 1987).

147 The objective of this study was to develop improved temperature, precipitation and vapour
148 pressure datasets for Bhutan that address limitations of existing climate surfaces available for
149 the region. This was done by using the local weather station network in conjunction with
150 spline-based interpolation methods. The relative performance improvements that can be
151 achieved by including thermal remote sensing data and local topographic metrics as partial
152 spline dependencies when interpolating temperature variables were also assessed. These
153 variables have recently demonstrated an improvement in temperature interpolation
154 performance in topographically complex landscapes in southeast Australia (Stewart &
155 Nitschke 2016). The climate surfaces developed in this study were compared against the
156 globally representative WorldClim (Hijmans et al. 2005) and CRU CL 2.0 (New et al. 2002)
157 datasets in order to highlight the importance of spatial resolution and observation density
158 when developing interpolated climate surfaces.

159

160 **Method**

161 ***Study Site***

162 Bhutan is a land-locked country located on the southern slopes of the eastern Himalayas,
163 sharing borders with China to the north and India to the east, west and south. The largely
164 mountainous country is 38,394 km^2 in area and ranges from approximately 100 m asl in the
165 south to 7,500 m asl in the far north (Figure 2). The extreme range in elevation leads to
166 highly variable climatic conditions within a distance spanning only 170 km in latitude (Norbu
167 et al. 2003). Like many regions of Asia the climate of Bhutan is monsoonal. South-westerly
168 winds bring moist air from the Bay of Bengal to Bhutan during the summer phase of the
169 north Indian monsoon (Krishnamurti et al. 2013; Tamang 2014). The country has three
170 distinct climatic zones; alpine, temperate and subtropical (NSB 2015). The climate is humid
171 and subtropical in the southern plains and foothills (100 – 2,000 m asl), with heavy rainfall

occurring during the summer monsoon. The inner Himalayan valleys of the central regions have a temperate climate (2,000 – 4,000 m asl); however, they often receive less rainfall than the surrounding slopes and ridges as cloud cover and precipitation are suppressed by strong up-valley and up-slope winds (Barry 2008; Whiteman 2000). The high Himalayas to the north experience a cold alpine climate (4,000 m asl and above) and a permanent snow line can be found above 4,800 m asl (Tamang 2014). In winter, the snow line across the eastern Himalayas can descend to around 3,000 m asl (Mani 1981).

The estimated population of Bhutan is 784,000 (as of 2016), and approximately 56% of people are employed in the agricultural sector (NSB 2015; UN Data 2016). Over 70% of the country is under forest cover (Figure 3; LCMP 2011; NASA LP DAAC 2016). Bhutan hosts a diverse range of vegetation and forest types (Ohsawa 1987; LCMP 2011; NBSAP 2014), owing to the complex topography and corresponding climatic variability. The subtropical climate zone is comprised of broadleaf, chir pine (*Pinus roxburghii*) and tropical lowland forest. Fir, mixed conifer, blue pine (*Pinus wallichiana*) and mixed broadleaf and conifer forest can be found in the temperate climate zone, and the alpine climate zone consists of meadows and scrubs.

Datasets

Daily maximum temperature, minimum temperature, precipitation and relative humidity records for 71 weather stations operating between January 1986 and December 2015 were obtained from the Department of Hydro-Met Services (DHMS), Ministry of Economic Affairs, Bhutan. Latitude, longitude and elevation at each station were extracted from site metadata also provided by the DHMS. The network of stations used throughout the analysis was distributed across elevations ranging from 180 m asl to 3,537 m asl (Figure 1). The record length at each station was on average 19.6 years long, with a minimum of 6.7 years

and maximum of 30 years of observations. Daily records were excluded where the maximum temperature was reported as lower than the minimum temperature (795 daily records), relative humidity was below 0 % or above 100 % (128 daily records), or the amount of precipitation was negative (7 daily records).

Estimates of daily vapour pressure, rather than observations of relative humidity, were used to ensure dependence upon elevation. Daily vapour pressure was derived from the saturation vapour pressure of the mean daily temperature and relative humidity (Abtew & Melesse 2013). The mean daily temperature was calculated as the average of the maximum and minimum temperature. The saturation vapour pressure, e_s , was calculated using a reparameterisation (Alduchov & Eskridge 1996) of the August-Roche-Magnus equation (Lawrence 2005);

$$e_s(T) = 6.1094 \times exp^{\frac{17.625 \times T}{243.04+T}} \quad (1)$$

The daily vapour pressure, e, was then derived from the saturation vapour pressure at the mean temperature and relative humidity (RH);

$$e = e_s(T_{mean}) \times RH \quad (2)$$

Provisional climate normals (hereafter referred to as climate normals), representing the mean monthly conditions between 1986 and 2015, were calculated for maximum temperature, minimum temperature, precipitation and vapour pressure at each station. Monthly values were computed using daily observations prior to the calculation of mean monthly values. Monthly precipitation was calculated as the sum of daily precipitation where observations were available for each day of the month. Monthly mean temperature and vapour pressure

were calculated as the mean of each daily observation where the following criteria were met; (1) no more than 10 missing days of data were allowed, and (2) no more than 4 consecutive days of missing data were allowed (WMO 2011). Calculating climate normals for any reference period may be biased due to short or incomplete records at different observation locations. A regression patching approach was tested to correct for any potential bias induced by short term records by regressing observations against neighbouring stations (Hopkinson et al. 2012; Stewart & Nitschke 2016); however, this method did not produce reliable results. Monthly climate normals were therefore calculated for each station where at least 10 years of observations were available for each month (Hijmans et al. 2005) to ensure interpolation was supported by a sufficient number of data points in different locations and at the highest elevations.

Potential biases in short term means were investigated using interpolation variance and by analysing ranked residuals throughout the cross validation procedure for each variable. Stations were identified as suspect where the calculated mean value was more than 3.6 standard deviations from the cross validated prediction. This approach identified one suspect station which was subsequently removed from all analysis due to close proximity with neighbouring stations and short record length (10 years for each month). The removal of additional short term records selected based on ranked residuals consistently led to decreased performance at neighbouring stations (including those with more than 20 years of data) and therefore they were retained throughout the analysis. Excluding the suspect station and those with less than 10 years of data resulted in a satisfactory spatial and temporal coverage, with the number of stations available for analysis reduced by between 6 and 11 % for any variable or month.

246 The digital elevation model (DEM) used throughout the analysis was obtained from the
247 CGIAR Consortium for Spatial Information (http://srtm.csi.cgiar.org). This was resampled to
248 7.5 arc seconds (approx. 225 m cell resolution at the equator) using the sink-filled 3 arc
249 second (approx. 90 m cell resolution) Shuttle Radar Topography Mission (SRTM) dataset
250 (Jarvis et al. 2008). One of the issues with interpolating precipitation across a fine resolution
251 DEM is that the predictions are heavily influenced by local topography, leading to
252 unrealistically large differences at very small spatial scales. As precipitation is not strongly
253 correlated with elevation at distances up to 5 km to 10 km (Hutchinson 1998; Sharples et al.
254 2005), the original DEM was smoothed using a Gaussian filter for calibrating and predicting
255 precipitation (Barnes 1964; Daly et al. 2007). The use of a focal filter to smooth elevation
256 allows for precipitation surfaces to be generated at high resolution without extreme short
257 range variability. The degree of smoothing is determined by the filter extent and standard
258 deviation of the Gaussian distribution. The smoothing filter was applied with a circular search
259 diameter of 35 cells (approx. 7.8 km) and a standard deviation of 10 cells using the System
260 for Automated Geoscientific Analysis (SAGA) software package (Conrad et al. 2015). The
261 required level of smoothing was determined by iteratively adjusting the standard deviation of
262 the filter (5 to 25) and cross validating precipitation climate normals (Appendix S1).
263 Performance was optimal at a standard deviation of 10 cells, although the differences
264 between each level of smoothing varied by less than 1.5% in RMSE. Geographic coordinates
265 were expressed in decimal degrees and elevation expressed in kilometres during all analyses
266 (Hutchinson 1995; Hutchinson 1998; Hutchinson 2009) to minimise error during cross
267 validation and surface generation.

268

269 The effects of topographic position on minimum temperature were assessed using a
270 topographic index of relative elevation, which has been shown to improve model

271 performance by representing the effect of overnight temperature inversions and cold air
272 pooling processes (Daly et al. 2007; Ashcroft & Gollan 2012; Stewart & Nitschke 2016).
273 This index was calculated as the square root of the difference between the elevation at each
274 target cell and focal minimum within an 8.76 km circular search diameter. The optimal focal
275 range for the topographic index was systematically assessed by iteratively adjusting the
276 search diameter (1.1 km to 90.2 km) and cross validating minimum temperature (Appendix
277 S2).
278
279 Thermal remote sensing data from collection 6 of the Moderate Resolution Imaging
280 Spectroradiometer (MODIS) MOD11A2 (Wan et al. 2015) Land Surface Temperature (LST)
281 product (approx. 1 km cell resolution) was used as an independent covariate for temperature
282 interpolation. The MOD11A2 MODIS product can be effective in improving temperature
283 interpolation (Hengl et al. 2012; Stewart & Nitschke 2016) as it provides an indirect estimate
284 of land surface temperature and is sensitive to land cover classification (Snyder et al. 1998;
285 Wan 2006). All 8-day composite scenes available between February 2000 and December
286 2015 were downloaded using the *MODIS* package (Mattiuzzi 2016) in R (R Core Team
287 2016). Scenes were rejected where visual inspection indicated clear spatial artefacts, or the
288 number of cells with invalid LSTs was greater than 50% across Bhutan. This threshold was
289 set to ensure enough scenes were retained during the summer monsoon, when there is a very
290 high level of cloud cover. Each image was then transformed into z-scores, grouped by month
291 and averaged for each cell location. Outliers falling outside of the 95% confidence interval
292 were excluded when calculating the final mean value at each cell location (Stewart &
293 Nitschke 2016). Standardised monthly MODIS surfaces were calculated separately for day
294 scenes and night scenes to be used as predictors for interpolation of maximum temperature
295 and minimum temperature, respectively. Due to the extremely cloudy conditions and spatial

296 artefacts noted for several months during visual inspection of the LSTs, clear sky masks from
297 the MOD11A2 product were also used to support the analysis. Daily clear sky images were
298 extracted by converting 8-bit integers in the 8-day composite clear sky data to binary vectors.
299 The mean fraction of clear sky during the day and night was then calculated for each pixel,
300 and as a regional average, for each month.

301

302 ***Data Analysis***

303 Monthly maximum temperature, minimum temperature, precipitation and vapour pressure
304 climate normals for the 1986-2015 reference period were interpolated using trivariate splines
305 (Wahba 1990; Hutchinson 1995) in ANUSPLIN 4.4 (Hutchinson & Xu 2011). The spline
306 smoothing parameter was estimated using generalised cross validation (GCV; Craven &
307 Wahba 1979). For each variable, full spline dependence upon latitude, longitude and
308 elevation was assessed. Additional partial dependencies (Bates et al. 1987) were also assessed
309 for both maximum temperature (standardised MODIS day time LST) and minimum
310 temperature (standardised MODIS night time LST, topographic index). The square root of
311 vapour pressure (McKenney et al. 2004) and precipitation (Hutchinson 1995; Hutchinson
312 1998; Hutchinson 2009) climate normals were used for interpolation and the final predictions
313 were subsequently converted back to units of hectopascals (hPa) and millimetres.
314 ANUSPLIN internally corrects for the small amount of bias that arises as a result of these
315 transformations (Hutchinson & Xu 2011). As site elevations extracted from the smoothed
316 precipitation DEM are a function of the surrounding landscape they may differ from values
317 present in the site metadata (RMSE = 323 m). Precipitation was therefore cross validated
318 using both the actual and smoothed elevation values to ensure the smoothed interpolation
319 would produce reliable results.

320

Cross validation was performed by iteratively leaving out one observation and refitting the model until independent predictions were made for all locations. The coefficient of determination (r^2), mean absolute error (MAE), root mean square error (RMSE), ratio of the RMSE to the standard deviation of the observations (RSR; Moriasi et al. 2007) and mean error (BIAS) were used to assess model performance. Following cross validation, monthly climate normal surfaces were generated using all available stations for each model.

Residual analyses were performed to investigate the differences in model predictions when using alternative variables for interpolation, and also to compare the surfaces generated in this study against globally representative climate datasets. In order to detect differences in the spatial distribution of model predictions for temperature, residual values were calculated for each partial trivariate spline model by subtracting the trivariate spline with full dependence upon latitude, longitude and elevation. Empirical cumulative distribution plots were used to investigate the spread of mean annual maximum and minimum temperature residuals. November was selected to illustrate the spatial distribution of minimum temperature residuals.

Mean annual temperature and annual precipitation were extracted from the WorldClim (Hijmans et al. 2005) and the CRU CL 2.0 (New et al. 2002) datasets and compared against the new surfaces generated using the local weather station network. Residuals were calculated by subtracting the WorldClim and CRU surfaces from the gridded datasets generated in this study. Thermal remote sensing data is sensitive to land use type (Snyder et al. 1998; Wan 2006) and therefore partial spline models for temperature using standardised MODIS LST values were not assessed against the WorldClim or CRU datasets to ensure an appropriate comparison.

Results

Cross validated statistics for maximum temperature, minimum temperature, vapour pressure and precipitation climate normals are summarised in Table 1. All partial spline models for temperature variables provided a performance improvement over the full trivariate spline. Pooled statistics for maximum temperature demonstrate a 7.9 % improvement in RMSE over the full trivariate spline when using standardised day time MODIS LST values as an independent covariate. Pooled statistics for minimum temperature demonstrate an improvement of between 10.4 % and 12.3 % in RMSE when using standardised night time MODIS LST values, the topographic index, or their combination, as independent covariates. The use of smoothed DEM values rather than site elevations provided an 8.8% reduction in RMSE for precipitation. All variables achieved an RSR of 0.3 or less, indicating good model performance. Mean error (BIAS) was negligible for temperature and vapour pressure; however, there was a small negative bias for smoothed precipitation (-5.01 mm) which equated to -0.03 % as a proportion of the mean observed value.

The cross validated monthly RMSE for all variables and models summarised in Table 1 are illustrated in Figure 4. The partial trivariate spline for maximum temperature (3DS-M) was effective throughout the year and demonstrated the largest improvement between January and October (4.8% to 16.0% reduction in RMSE) when compared against the full trivariate spline (3DS). Partial spline models for minimum temperature (3DS-T, 3DS-M and 3DS-TM) were most effective in improving performance during the cooler months between October and April; however, they also provided a small improvement in May. Minimum temperature typically performed best during this period when including partial dependence upon both the standardised MODIS values and the topographic index (3DS-TM; 10.4% to 23.4% reduction

371 in RMSE when compared against 3DS). The RMSE of monthly precipitation climate normals
372 cross validated using the full trivariate spline (3DS) was highest during the wettest months
373 between May and September (RMSE between 55.8 mm and 120.7 mm). The ratio of the
374 RMSE to the mean was relatively stable across this period (29.3% to 37.1%), suggesting that
375 the high RMSE values are likely due to increased precipitation rather than reduced model
376 performance.

377

378 Daily MODIS acquisitions show that the fraction of clear sky over Bhutan is lowest during
379 the day between May and September (Figure 5). The regional mean vapour pressure is also
380 highest during these months. With the exception of May, partial spline models were
381 ineffective at improving minimum temperature interpolation performance throughout this
382 period when compared against the trivariate spline with full dependence upon latitude,
383 longitude and elevation. The clear sky fraction was on average lower during the night
384 between October and April.

385

386 The distribution of mean annual maximum and minimum temperature residuals, calculated by
387 subtracting the full trivariate spline (3DS) from each partial trivariate spline variant (3DS-T,
388 3DS-M and 3DS-TM), are presented in Figure 6. Mean annual maximum temperature
389 residuals (3DS-M) range from -4.2 °C to 4.8 °C and are cooler than the full trivariate spline
390 across 81.2 % of the region. Mean annual minimum temperature residuals (Figure 6)
391 demonstrate congruence between the partial trivariate spline models and are warmer across
392 68.2 % of cells for 3DS-T (-2.2 °C to 1.9 °C), 71.9% of cells for 3DS-M (-2.3 °C and 3.0 °C),
393 and 73.1% of cells for 3DS-TM (-2.1 °C and 2.6 °C).

394

Minimum temperature residuals in November (Figure 7) show a similar spatial distribution for all models, with a warming of slopes and cooling of areas with low relative elevation. Minimum temperature interpolation using standardised MODIS LST values show a much broader range of values in comparison to variants using only topographic metrics. Residuals were up to 1.8 °C cooler and 1.3 °C warmer for 3DS-TM in comparison to the maximum range predicted by 3DS-T.

The spatial distribution of mean annual temperature and annual precipitation interpolated using the local weather station network (maximum temperature 3DS; minimum temperature 3DS-T; precipitation 3DS) show large deviations from the WorldClim and CRU CL 2.0 datasets (Figure 8). The regional mean annual temperature for locally calibrated interpolations was 0.75 °C warmer than the WorldClim dataset, and 1.81 °C warmer than the CRU dataset. This result was most pronounced across the western regions of Bhutan in the WorldClim dataset. For mean annual temperature, the residuals between the new surfaces and the WorldClim values varied by as much as 5.9 °C and the residuals between the new surfaces and the CRU values varied by up to 12.9 °C. The 3DS model predicts the greatest amount of precipitation across the southern foothills of Bhutan; however, unlike the WorldClim and CRU datasets, these high rainfall regions do not extend into the central valleys. Precipitation residuals show deviations of up to 3,364 mm in the WorldClim dataset, and up to 2,845 mm in the CRU dataset when compared against locally calibrated interpolation. Precipitation typically decreases with elevation across Bhutan in the WorldClim and CRU datasets. The 3DS model exhibits an increase in precipitation with elevation across the central valleys and a decrease in overall precipitation towards the far north of Bhutan.

Discussion

The results of this study demonstrate the advantages of incorporating MODIS LST data and local topographic indices as additional partial dependencies when interpolating temperature variables across topographically complex landscapes, such as those in Bhutan. Stewart and Nitschke (2016) found similar outcomes for the effectiveness of these variables in southeast Australia, despite large differences in topographic and climatic conditions. They found that MODIS LST values improved maximum temperature interpolation performance the most during the warm summer months. In Bhutan, the largest improvements in maximum temperature interpolation performance were also achieved during the warmest months when using standardised MODIS LST values as an independent covariate. This performance improvement was maintained throughout the summer monsoon, despite heavy day time cloud cover which reduced the amount of data available to construct standardised surfaces. The MOD11A2 product is sensitive to land cover classification, and therefore the seasonal performance differences may be due to the indirect detection of spatially aggregated microclimatic conditions responding to higher temperatures, particularly during the summer months.

Both the MODIS LST values and local topographic metrics were effective at improving minimum temperature interpolation performance during the dry months between October and May; however, neither provided a performance improvement between June and September. This congruence suggests that MODIS LST data may be particularly effective at detecting temperature inversion signals in the long term climate record, and also indicates that the effectiveness of these variables may be considerably reduced during cloudy, wet and humid conditions that are characteristic of the summer monsoon in Bhutan. The extensive cloud cover observed during these months did not have a negative impact on maximum temperature

445 performance when using MODIS LST values, and therefore the lack of performance
446 improvement for minimum temperatures was likely due to the absence of a detectable
447 inversion effect in the long term record, rather than as a result of poor data quality. The
448 release of latent heat and suppression of outgoing longwave radiation associated with
449 extensive cloud cover, heavy precipitation and high vapour pressure are likely to overcome
450 the influence of temperature inversions and local topography during the wet months of the
451 summer monsoon. These conditions are likely to suppress temperature inversion regimes due
452 to their influence upon the surface energy balance (Iijima & Shinoda 2000; Whiteman et al.
453 2007; Barry 2008; Zardi & Whiteman 2013). The nocturnal release of latent heat has also
454 been associated with the persistence of up-slope and up-valley winds in the eastern
455 Himalayas (Ohata et al. 1981; Barry 2008), which may further suppress thermal stratification
456 of air near the surface and the development of cold air flows and pools. Both variables were,
457 however, effective at improving minimum temperature interpolation performance between
458 October and May. When included separately as partial dependencies, each variable led to a
459 warming of slopes and a cooling of valley bottoms when compared against the trivariate
460 spline with full dependence upon latitude, longitude and elevation. This result is consistent
461 with the current understanding of nocturnal temperature distributions in mountainous terrain
462 (Geiger 1965; Whiteman 2000; Barry 2008).

463

464 Horizontal scaling of the topographic index resulted in an optimal search diameter of
465 approximately 8.8 km, which is 5 times greater than the optimal diameter identified for
466 southeast Australia (Stewart & Nitschke 2016). Furthermore, using both MODIS LST data
467 and the topographic index provided an additive improvement in minimum temperature
468 performance in southeast Australia that was not found for Bhutan. This is potentially due to
469 the scale of topographic variation in Bhutan (southeast Australia is comparatively much

flatter with small peak-to-peak distances in the alpine regions) and the ability of the MODIS LST data to detect temperature inversions at appropriate scales. These results suggest that a spatially varying dependence upon the topographic index, calculated with short search diameters, in conjunction with MODIS LST data may allow for spatial interpolation of current minimum temperatures at much greater spatial extents. This may prove useful for spatial predictions of current climate; however, thermal remote sensing data is sensitive to land cover and therefore should not be used for projecting climate change scenarios.

When utilising the local weather station network in Bhutan, new precipitation surfaces were able to characterise the heavy rainfall experienced in the southern foothills while retaining the effect of orography on precipitation throughout the central valleys and ranges. Precipitation is suppressed across the interior of these valleys and ranges by strong up-valley and up-slope winds (Whiteman 2000), which can lead to an underestimation of rainfall throughout the central regions of Bhutan (Norbu et al. 2003). Historical rainfall data and the distribution of vegetation suggests that the slopes and ridges throughout these regions are wetter than the inner valleys (Ohsawa 1987; Norbu et al. 2003), which is reflected in the spatial distribution of precipitation predicted in this study. The precipitation surfaces presented should be interpreted with a degree of caution, as much of the precipitation in the higher elevation regions of Bhutan falls as snow and elevations above 3,537 m asl are not represented by the local weather station network. Furthermore, precipitation is highly variable in the southern foothills of Bhutan and the representativeness of mean conditions is therefore dependent upon the available data series length.

The importance of spatial resolution and observation density is apparent when comparing the datasets developed as part of this study against globally consistent climate datasets such as

WorldClim and CRU CL 2.0. Analyses of the CRU CL 2.0 residuals show that the within-cell mean annual temperature variability can be as high as 20 °C for coarse resolution products in Bhutan. While downscaling approaches are an option, they cannot incorporate the effects of mesoscale processes such as temperature inversions. The temperature bias that is evident in the WorldClim residuals across western Bhutan, where temperatures are often at least 2.5 °C cooler than predicted in the present study, indicate the importance of observation density and placement. It is unlikely that this region has experienced such an increase in mean annual temperature given that the datasets compared are centred on reference periods that differ by only 25 years. The analyses of precipitation residuals show extreme deviations between the present study and both the WorldClim and CRU CL 2.0 datasets. These results support conclusions by Hijmans (et al. 2005) that station density is perhaps the most important factor for inferring the quality of interpolated climate datasets. Station observations that qualify for inclusion in global databases may be limited in many cases due to data and weather station availability, insufficient length of records, or lack of quality control processes. When globally representative surfaces such as WorldClim are used for regional studies, an evaluation of point density and topographic variability is recommended to evaluate whether or not these surfaces are likely to capture climatological processes at appropriate scales. Acquisition and interpolation of regional weather station data may be justified, and in some cases required, where the point density is too low.

The temperature and vapour pressure surfaces generated as part of this study allow for the spatial estimation of vapour pressure deficit and relative humidity. These variables can be critical for modelling vegetation distributions, as they characterise the atmospheric demand for moisture. While outside the scope of the present study, vapour pressure surfaces may also be used for atmospheric attenuation when modelling potential incoming solar radiation (e.g.

Böhner & Antoni 2009; Conrad et al. 2015). Vapour pressure precludes the need for estimates of lumped atmospheric transmittance, and allows for the effects of elevation to be incorporated into solar radiation predictions. Solar radiation modelling in Bhutan is, however, likely to be complicated by heavy cloud cover, particularly during the summer monsoon. Observations of sunlight hours are available at a small number of stations within the local weather station network in Bhutan, which may facilitate the production of high quality solar radiation surfaces in the future.

Conclusion

The datasets presented in this paper provide a new resource for ecological and agricultural research in Bhutan. Alternative versions of temperature variables were generated to provide the highest quality surfaces (MODIS LST variants) and to maximise compatibility with climate change projections (topographic index). These temperature datasets are calibrated specifically for Bhutan using the local weather station network, are sensitive to the climatic conditions present during the summer monsoon, and incorporate inversion signals that cannot be detected using existing methodologies for statistical downscaling. Both the topographic index and the standardised night time MODIS LST values show evidence that they can detect the effects of temperature inversions on minimum temperature climate normals. These particular covariates are rarely used to improve temperature interpolation, and therefore their application is novel for the region. Precipitation surfaces characterise the heavy precipitation observed in the southern foothills, while retaining the effects of orography throughout the central regions of Bhutan. These effects are absent from global climate surfaces as they do not include weather station observations from within Bhutan. Incorporating the effect of orography on precipitation using trivariate spline interpolation provides a large improvement over polynomial regression techniques that have previously been applied in Bhutan. Globally

545 representative humidity data is very coarse in resolution. The inclusion of vapour pressure
546 surfaces allows for the calculation of humidity metrics and vapour pressure deficit, which
547 will further facilitate ecological modelling and assist in decision making for climate change
548 adaptation throughout Bhutan.

549

550 **Acknowledgements**

551 We would like to thank the Department of Hydro-Met Services (DHMS), Ministry of
552 Economic Affairs, Bhutan, for providing weather station data which made this research
553 possible. The research was supported by the Melbourne Research Scholarship (University of
554 Melbourne) with additional funding provided by the State of Victoria Department of
555 Environment, Land, Water and Planning (DELWP) though the Integrated Forest Ecosystem
556 Research (iFER) program.

557

558 **References**

559 Abtew W, Melesse A. 2013. Vapour pressure calculation methods. In: Evaporation and
560 evapotranspiration: measurements and estimations. Springer: Netherlands. doi:
561 10.1007/978-94-007-4737-1.

562 Alduchov OA, Eskridge RE. 1996. Improved Magnus form approximation of saturation
563 vapour pressure. *Journal of Applied Meteorology* **34(4):** 601-609. doi: 10.1175/1520-
564 0450(1996)035<0601:IMFAOS>2.0.CO;2.

565 Ashcroft MB, Gollan JR. 2012. Fine-resolution (25 m) topoclimatic grids of near-surface (5
566 cm) extreme temperatures and humidities across various habitats in a large (200 / x 300
567 km) and diverse region. *International Journal of Climatology* **32(14):** 2134-2148.

doi:10.1002/joc.2428.

Austin MP, Van Niel KP. 2011. Improving species distribution models for climate change studies: variable selection and scale. *Journal of Biogeography* **38(1):** 1-8. doi: 10.1111/j.1365-2699.2010.02416.x.

Barnes SL. 1964. A technique for maximizing details in numerical weather map analysis. *Journal of Applied Meteorology* **3(4):** 396-409. doi: 10.1175/1520-0450(1964)003<0396:ATFMDI>2.0.CO;2.

Barry RG. 2008. Mountain weather and climate. Cambridge University Press: Cambridge, United Kingdom. doi: 10.1017/CBO9780511754753.

Bates DM, Lindstrom MJ, Wahba G, Yandell BS. 1987. GCVPACK–routines for generalized cross validation. *Communications in Statistics-Simulation and Computation* **16(1):** 263-297.

Bonan GB, Levis S, Kergoat L, Oleson, KW. 2002. Landscapes as patches of plant functional types: an integrating concept for climate and ecosystem models. *Global Biogeochemical Cycles* **16(2)**. doi: 10.1029/2000GB001360

Böhner J, Antoni O. 2009. Chapter 8: Land-surface parameters specific to topo-climatology. *Developments in Soil Science* **33:** 195-226. doi:10.1016/S0166-2481(08)00008-1.

Climatic Research Unit (CRU). 2016. *Land Stations used by the Climatic Research Unit within CRUTEM3*. University of East Anglia: Norwich, United Kingdom. https://crudata.uea.ac.uk/cru/data/landstations/. Accessed 1 August 2016.

Conrad O, Bechel B, Bock M, Dietrich H, Fischer E, Gerlitz L, Wehberg J, Wichmann V, Böhner J. 2015. System for automated geoscientific analyses (SAGA) v. 2.1.4. *Geoscientific Model Development* **8(7):** 1991-2007. doi: 10.5194/gmd-8-1991-2015.

Craven P, Wahba G. 1979. Smoothing noisy data with spline functions: Estimating the

592 correct degree of smoothing by the method of generalized cross-validation. *Numerische*
593 *Mathematik* **31:** 377-403.

594 Daly C, Smith JW, Smith JI, McKane RB. 2007. High-resolution spatial modelling of daily
595 weather elements for a catchment in the Oregon Cascade Mountains, United States.
596 *Journal of Applied Meteorology and Climatology* **46(10):** 1565–1586. doi:
597 10.1175/JAM2548.1.

598 Daly C, Conklin DR, Unsworth MH. 2009. Local atmospheric decoupling in complex
599 topography alters climate change impacts. *International Journal of Climatology* **30(12):**
600 1857-1864. doi: 10.1002/joc.2007.

601 Dorji U, Olesen JE, Bøcher PK, Seidenkrantz MS. 2016. Spatial variation of temperature and
602 precipitation in Bhutan and links to vegetation and land cover. *Mountain Research and*
603 *Development* **36(1)**: 66-79. doi: http://www.bioone.org/doi/10.1659/MRD-JOURNAL-
604 D-15-00020.1.

605 Elith J, Franklin J. 2013. Species Distribution Modeling. *Encyclopedia of Biodiversity* **6:**
606 692–705. doi:10.1016/B978-0-12-384719-5.00318-X.

607 Flohn H. 1970. Beiträge zur meteorologie des Himalaya. *Khumbu Himal.* **7(2)**: 25-45.

608 Friedl MA, Sulla-Menashe D, Tan B, Schneider A, Ramankutty N, Sibley A, Huang X. 2010.
609 MODIS collection 5 global land cover: algorithm refinements and characterization of
610 new datasets. *Remote Sensing of Environment* **114(1)**: 168-182. doi:
611 10.1016/j.rse.2009.08.016.

612 Geiger R. 1965. Climate near the ground. Harvard University Press: Cambridge,
613 Massachusetts, United States.

614 Harris I, Jones PD, Osborn TJ, Lister DH. 2014. Updated high-resolution grids of monthly
615 climatic observations – the CRU TS3.10 dataset. *International Journal of Climatology*

34(3): 623-642. doi: 10.1002/joc.3711.

Hengl T, Heuvelink GBM, Per ec Tadi M, Pebesma EJ. 2012. Spatio-temporal prediction of daily temperatures using time-series of MODIS LST images. *Theoretical and Applied Climatology* **107:** 265-277. doi:10.1007/s00704-011-0464-2.

Hijmans RJ, Cameron SE, Parra JL, Jones PG, Jarvis A. 2005. Very high resolution interpolated climate surfaces for global land areas. *International Journal of Climatology* **25(15):** 1965-1978. doi:10.1002/joc.1276.

Hijmans RJ, Cameron SE, Parra JL, Jones PG, Jarvis A. 2010. *WorldClim: global weather stations*. ESRI. https://www.arcgis.com/home/item.html?id=7644c6e78c1644b4bde2edfc44787520/. Accessed 1 August, 2016.

Hill SA. 1881. The meteorology of the north-west Himalaya. *Memoirs of the India Meteorological Department*. **1**: 377-429.

Hopkinson RF, Hutchinson MF, McKenney DW, Milewska EJ, Padadopol P. 2012. Optimizing input data for gridding climate normals for Canada. *Journal of Applied Meteorology and Climatology* **51**(8): 1508-1518. doi:10.1175/JAMC-D-12-018.1.

Hutchinson MF. 1995. Interpolating mean rainfall using thin plate smoothing splines. *International journal of geographical information systems* **9(4):** 385-403. doi:10.1080/02693799508902045.

Hutchinson, MF. 1998. Interpolation of rainfall data with thin-plate smoothing splines II: Analysis of topographic dependence. *Journal of Geographic Information and Decision Analysis* **2(2)**: 152-167.

Hutchinson MF, McKenney DW, Lawrence K, Pedlar JH, Hopkinson RF, Milewska E, Papadopol P. 2009. Development and testing of Canada-wide interpolated spatial

640 models of daily minimum-maximum temperature and precipitation for 1961 – 2003.
641 *Journal of Applied Meteorology and Climatology* **48(4):** 725-741.
642 doi:10.1175/2008JAMC1979.1.

643 Hutchinson MF, Xu T. 2013. ANUSPLIN Version 4.4 User Guide.

644 Iijima Y, Shinoda M. 2000. Seasonal changes in the cold-air pool formation in a subalpine
645 hollow, central Japan. *International Journal of Climatology* **20(12):** 1471-1483. doi:
646 10.1002/1097-0088(200010)20:12<1471::AID-JOC554>3.0.CO;2-6.

647 Jarvis A, Reuter HI, Nelson A, Guevara E. 2008. Hole-filled seamless SRTM data V4.
648 International Centre for Tropical Agriculture (CIAT). http://srtm.csi.cgiar.org.

649 Kattel DB, Yao T, Yang K, Tian L, Yang G, Joswiak D. 2013. Temperature lapse rate in
650 complex mountain terrain on the southern slope of the central Himalayas. *Theoretical*
651 *and Applied Climatology* **113:** 671-682. doi: 10.1007/s00704-012-0816-6.

652 Kattel DB, Yao T, Yang W, Gao Y, Tian L. 2015. Comparison of temperature lapse rates
653 from the northern to the southern slopes of the Himalayas. *International Journal of*
654 *Climatology* **35(15):** 4431-4443. Doi: 10.1002/joc.4297.

655 Krishnamurti TN, Stefanova , Misra V. 2013. Tropical meteorology. Springer: New York,
656 United States. doi: 10.1007/978-1-4614-7409-8.

657 Land Cover Mapping Project (LCMP). 2011. *Technical report: Bhutan land cover*
658 *assessment 2010 (LCMP-2010).* National Soil Services Centre (NSSC) and Policy and
659 Planning Division (PPD). Ministry of Agriculture and Forests. Royal Government of
660 Bhutan.

661 Lawrence M. 2005. The relationship between relative humidity and the dewpoint temperature
662 in moist air: a simple conversion and applications. *Bulletin of the American*
663 *Meteorological Society* **86(2):** 225-233. doi: 10.1175/BAMS-86-2-225.

Mani A. 1981. The climate of the Himalaya. In: Lall JS, Moddie AD (eds). The Himalaya: aspects of changes. Oxford University Press: New Delhi, India.

Mattiuzzi M. 2016. *MODIS: MODIS Acquisition and Processing*. R package version 0.10-34/r510. https://R-Forge.R-project.org/projects/modis/. Accessed 1 August, 2016.

McKenney DW, Hutchinson MF, Papadopol P, Price DT. 2004. Evaluation of alternative spatial models of vapour pressure in Canada. Proceedings: 26th Conference on Agricultural and Forest Meteorology. August 23-27. Vancouver, British Columbia. Natural Resources Canada, Great Lakes Forestry Centre.

Moriasi DN, Arnold JG, Van Liew MW, Bingner RL, Harmel RD, Veith TL. 2007. Model evaluation guidelines for systematic quantification of accuracy in watershed simulations. *Transactions of the ASABE* **50(3):** 885-900. doi:10.13031/2013.23153.

NASA LP DAAC. 2016. MCD12Q1 Land Cover Type Yearly L3 Global 500 m SIN Grid .V051. NASA EOSDIS Land Processes DAAC, USGS Earth Resources Observation and Science (EROS) Center: Sioux Falls, South Dakota (https://lpdaac.usgs.gov).

National Biodiversity Strategies and Action Plan of Bhutan (NBSAP). 2014. National Biodiversity Centre. Ministry of Agriculture and Forests. Royal Government of Bhutan.

National Oceanic and Atmospheric Administration (NOAA). 2016. Global historical climate network (GHCN). National Centres for Environmental Information: United States.

National Statistics Bureau (NSB). 2015. Statistical yearbook of Bhutan. National Statistics Bureau. Royal Government of Bhutan. http://www.nsb.gov.bt/.

New M, Hulme M, Jones, P. 1999. Representing twentieth-century space-time climate variability. Part I: Development of a 1961-90 mean monthly terrestrial climatology. *Journal of Climate* **12(3):** 829-856. doi:10.1175/1520-0442(1999)012<0829:RTCSTC>2.0.CO;2.

New M, Lister D, Hulme M, Makin I. 2002. A high-resolution data set of surface climate over global land areas. *Climate Research* **21(1):** 1–25. doi:10.3354/cr021001.

Norbu C, Baillie I, Dorji T, Dorj T, Tamang HB, Tshering K, Hutcheon A. 2003. A provisional physiographic zonation of Bhutan. *Journal of Bhutan Studies* **8:** 54-87.

Ohata T, Higuchi K, Ikegami K. 1981. Mountain-valley wind system in the Khumbu Himal, east Nepal. *Journal of the Meteorological Society of Japan*: 59(5): 753-762.

Ohsawa M. 1987. Vegetation zones in the Bhutan Himalaya. In: Ohsawa M (ed). Life zone ecology of the Bhutan Himalaya. Chiba University: Tokyo, Japan.

R Core Team, 2016. R: A language and environment for statistical computing. R Foundation for Statistical Computing: Vienna, http://www.R-project.org/.

Sharples JJ, Hutchinson MF, Jellet DR. 2005. On the horizontal scale of elevation dependence of Australian monthly precipitation. *Journal of Applied Meteorology* **44(12):** 1850-1865. doi: 10.1175/JAM2289.1.

Singh SP, Bassignana-Khadka I, Karky BS, Sharma E. 2011. *Climate change in the Hindu Kush-Himalayas: the state of current knowledge*. International Centre for Integrated Mountain Development (ICIMOD): Kathmandu, Nepal.

Snyder WC, Wan Z, Zhang Y, Feng Y-Z. 1998. Classification-based emissivity for land surface temperature measurement from space. International Journal of Remote Sensing 19(14): 2753-2774.

Stewart SB, Nitschke CR. 2016. Improving temperature interpolation using MODIS LST and local topography: a comparison of methods in south east Australia. *International Journal of Climatology*. doi: 10.1002/joc.4902.

Tamang TB. 2014. *Bhutan country presentation*. Regional Workshop on Implementation of Weather and Climate-related Services in the Least Developed Countries (LDCs) in Asia:

712 9-11 September, Thimphu, Bhutan.

713 Tse-ring K, Sharma E, Chettri N, Shrestha A (eds). 2010. Climate change vulnerability of
714 mountain ecosystems in the eastern Himalayas. International Centre for Integrated
715 Mountain Development (ICIMOD): Kathmandu, Nepal.

716 UN Data. 2016. *Country profile: Bhutan*. United Nations Statistics Division: New York,
717 United States. http://data.un.org/. Accessed 20 August, 2016.

718 Wahba G. 1990. *Spline models for observational data*. SIAM: Society for Industrial and
719 Applied Mathematics: Philadelphia, United States.

720 Wan Z. 2006. Collection-5 MODIS land surface temperature products users' guide.
721 http://www.icess.ucsb.edu/modis/LstUsrGuide/usrguide.html.

722 Wan Z, Hook S, Hulley G. 2015. MOD11A2 MODIS/Terra Land Surface
723 Temperature/Emissivity 8-Day L3 Global 1km SIN Grid V006. NASA EOSDIS Land
724 Processes DAAC, USGS Earth Resources Observation and Science (EROS) Center:
725 Sioux Falls, South Dakota (https://lpdaac.usgs.gov). doi:
726 10.5067/MODIS/MOD11A2.006.

727 Wang T, Hamann A, Spittlehouse DL, Murdock TQ. 2012. ClimateWNA—high-resolution
728 spatial climate data for Western North America. *Journal of Applied Meteorology and*
729 *Climatology* **51(1):** 16-29. doi:10.1175/JAMC-D-11-043.1.

730 Whiteman DC. 2000. Mountain meteorology: fundamentals and applications. Oxford
731 University Press: United Kingdom. ISBN: 0195132718.

732 Whiteman DC, De Wekker SFJ, Haiden T. 2007. Effect of dewfall and frostfall on nightime
733 cooling in a small, closed basin. *Journal of Applied Meteorology* **46:** 3-13. doi:
734 10.1175/JAM2453.1.

735 World Meteorological Organization (WMO). 2011. Guide to Climatological Practices.

WMO-No. 100. World Meteorological Organization: Geneva, Switzerland.

Zardi D, Whiteman DC. 2013. Diurnal mountain wind systems. In: Chow FK, De Wekker SFJ, Snyder BJS (eds). Mountain weather research and forecasting. Springer: New York, United States. doi: 10.1007/978-94-007-4098-3.

Zhisheng A, Kutzbach JE, Prell WL, Porter, SC. 2001. Evolution of Asian monsoons and phased uplift of the Himalaya-Tibetan plateau since late Miocene times. *Nature* **411**: 62-66. doi: 10.1038/35075035.

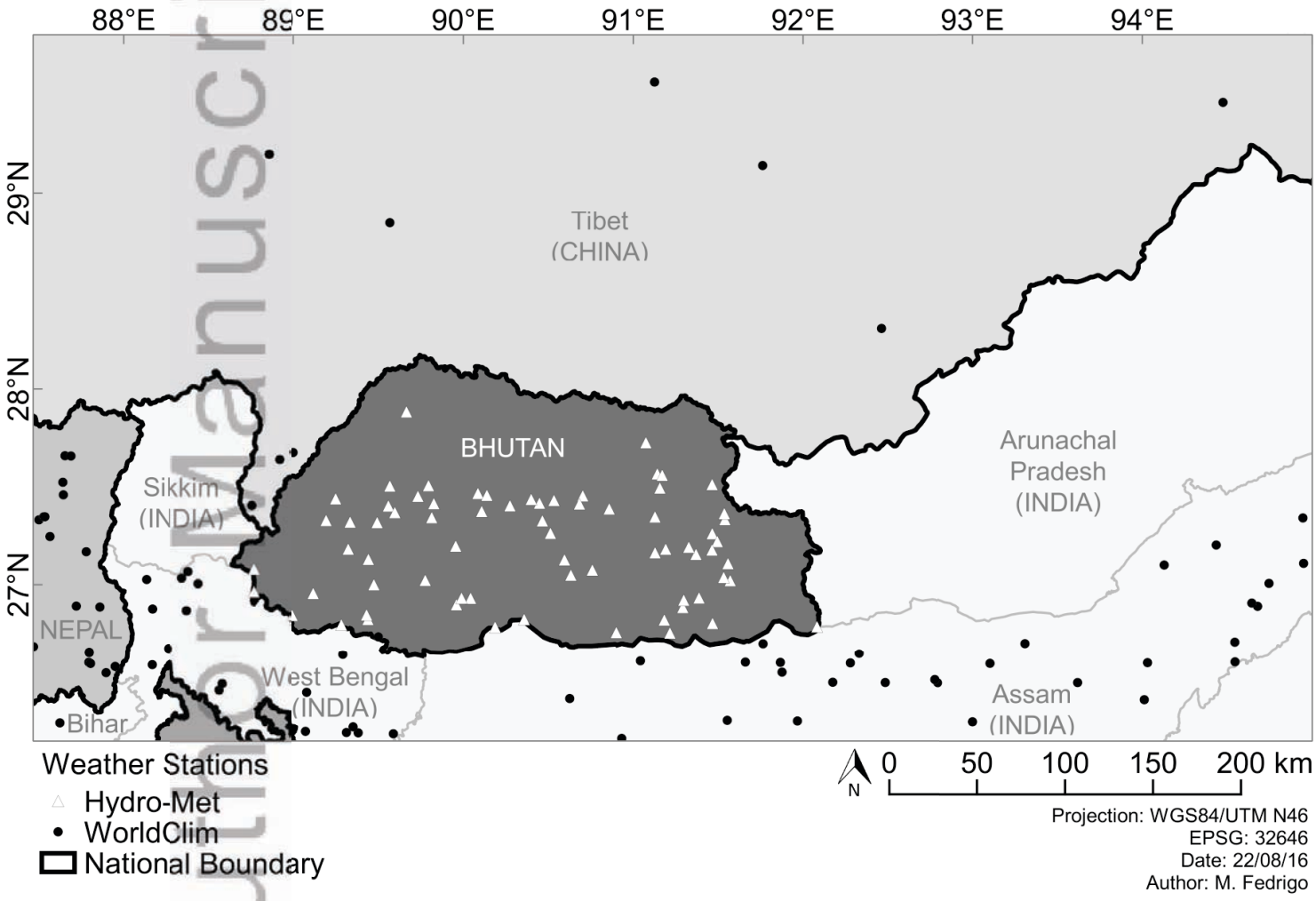

Figure1_WS_Locations.tif

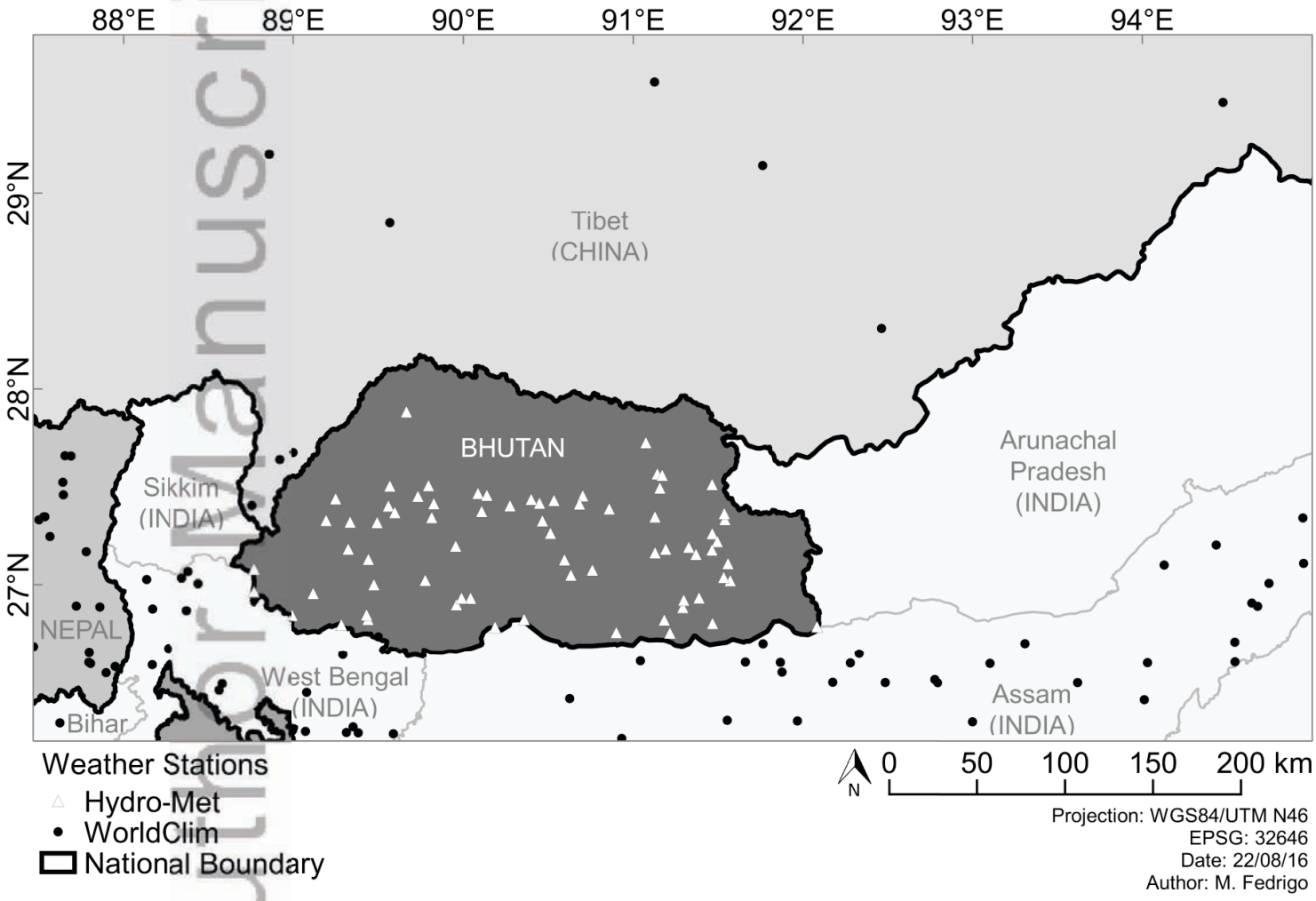

Figure1_WS_Locations.tif

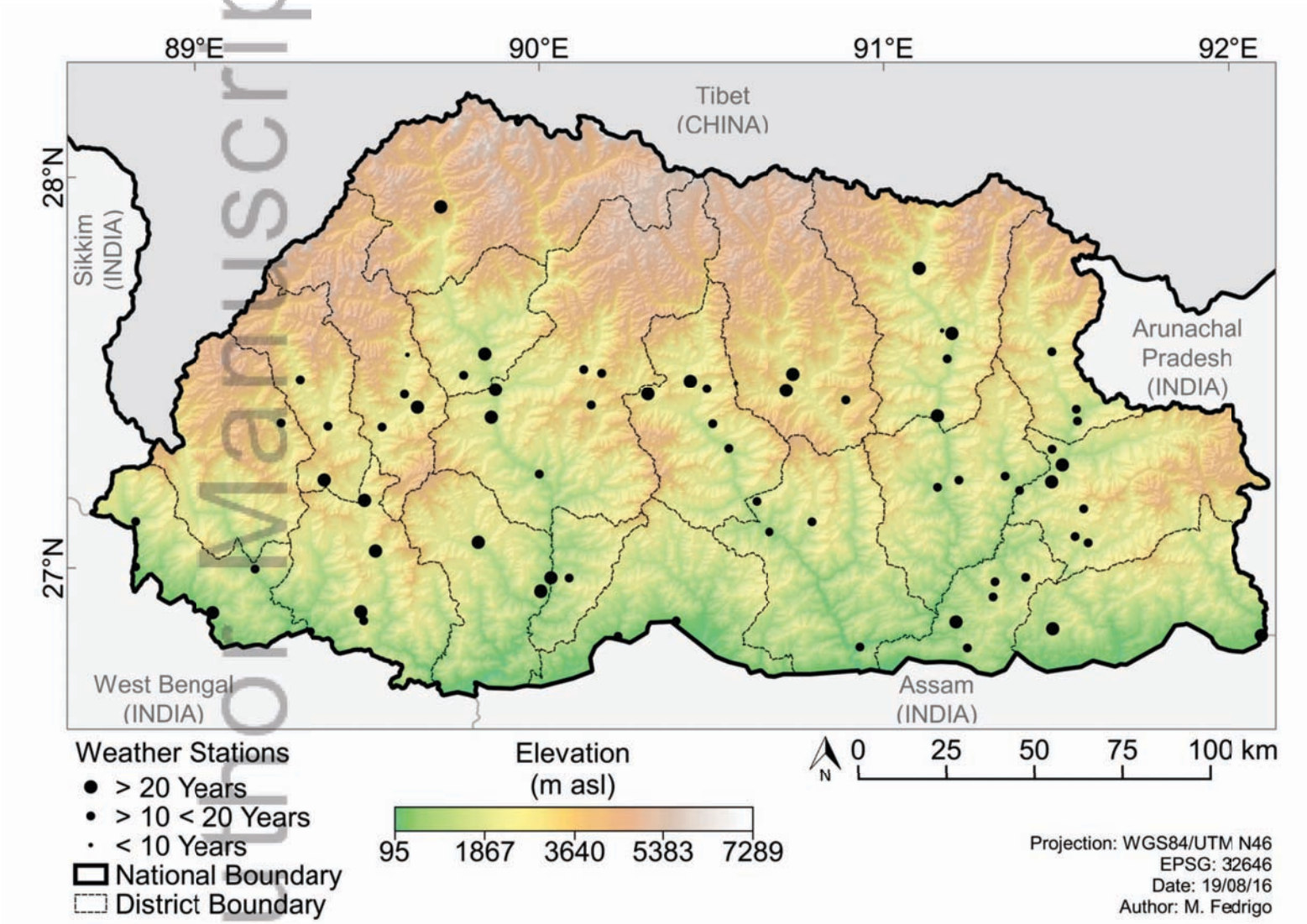

Figure2_DEM.tif

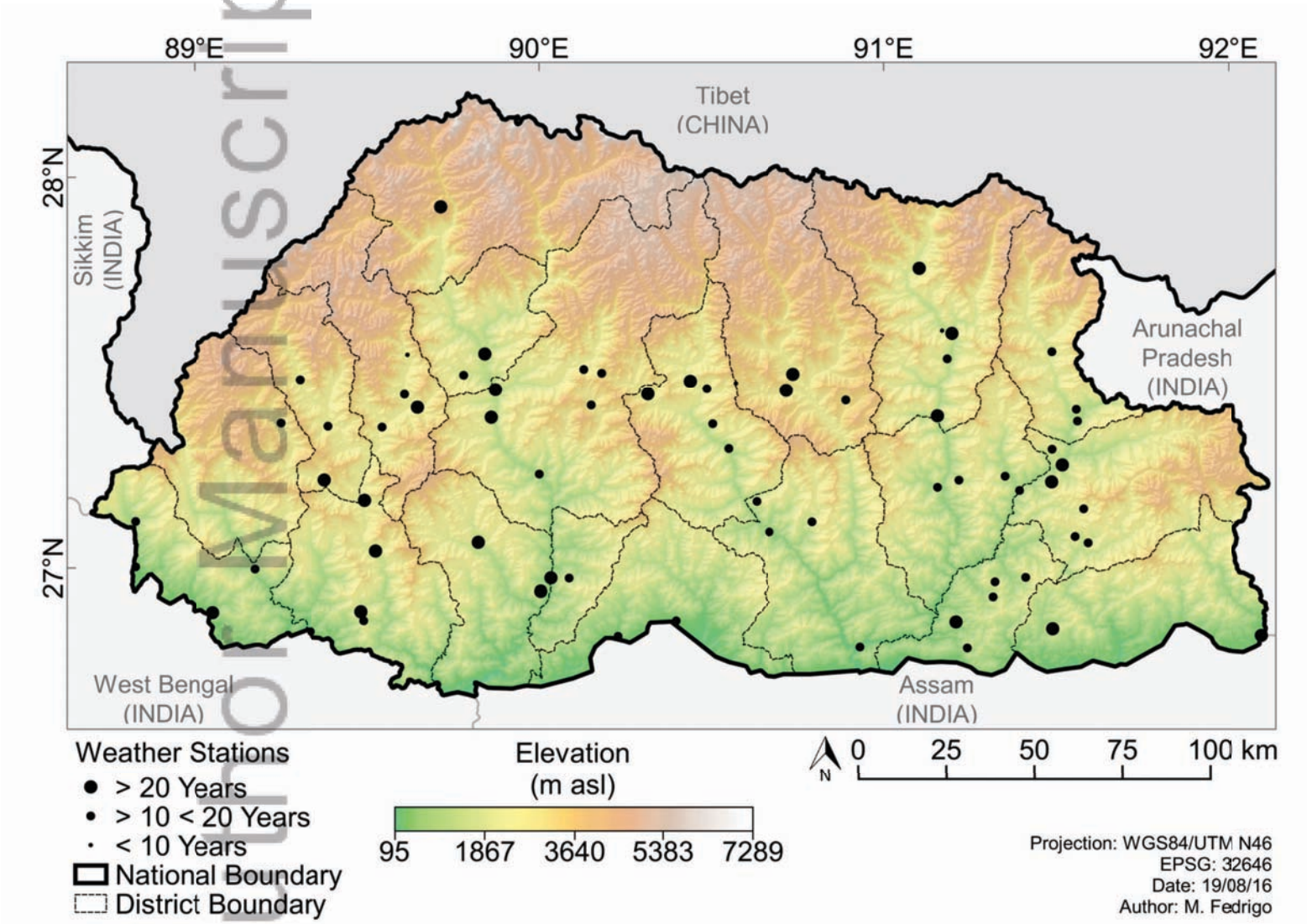

Figure2_DEM.tif

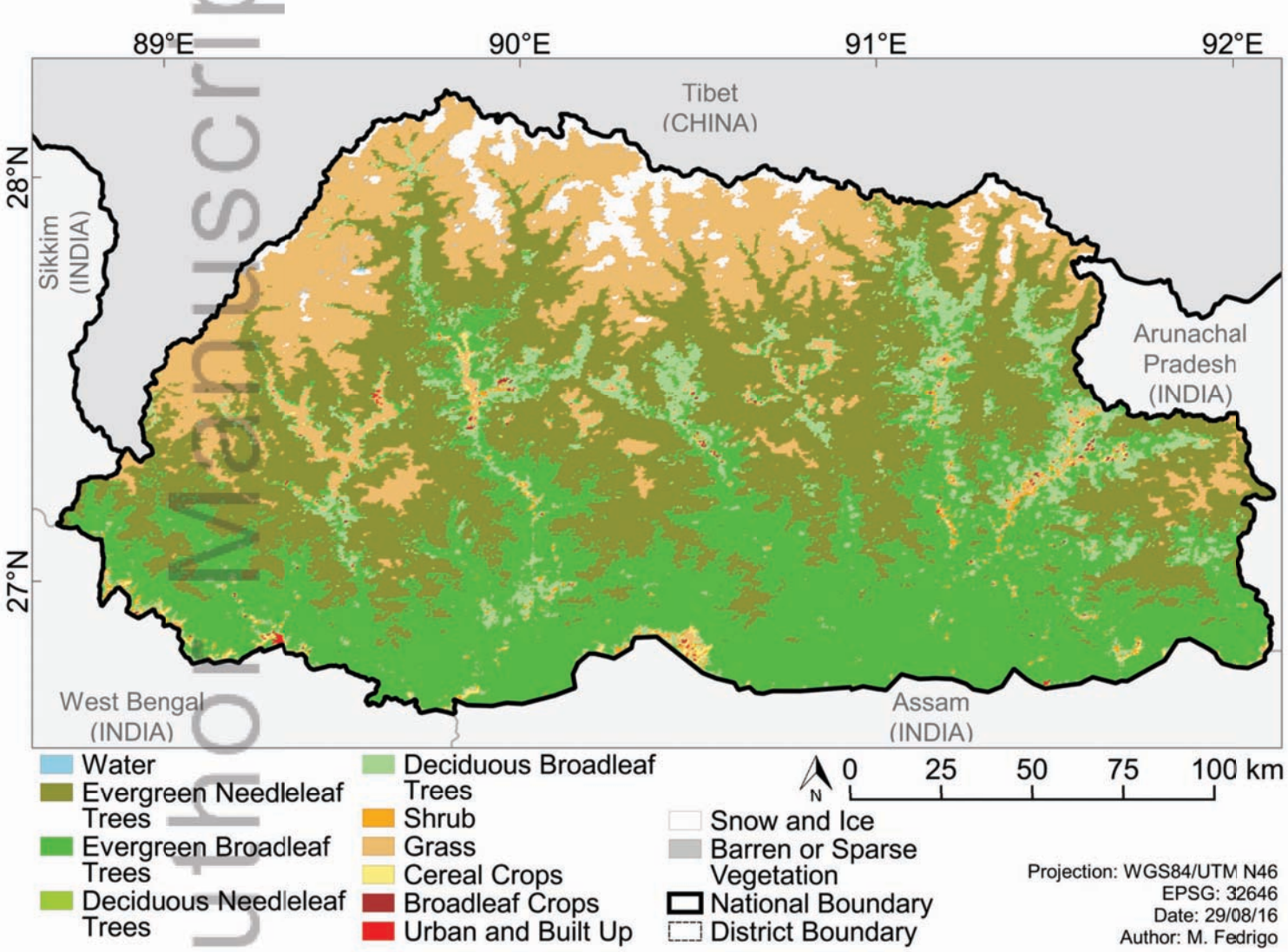

Figure3_LCC.tif

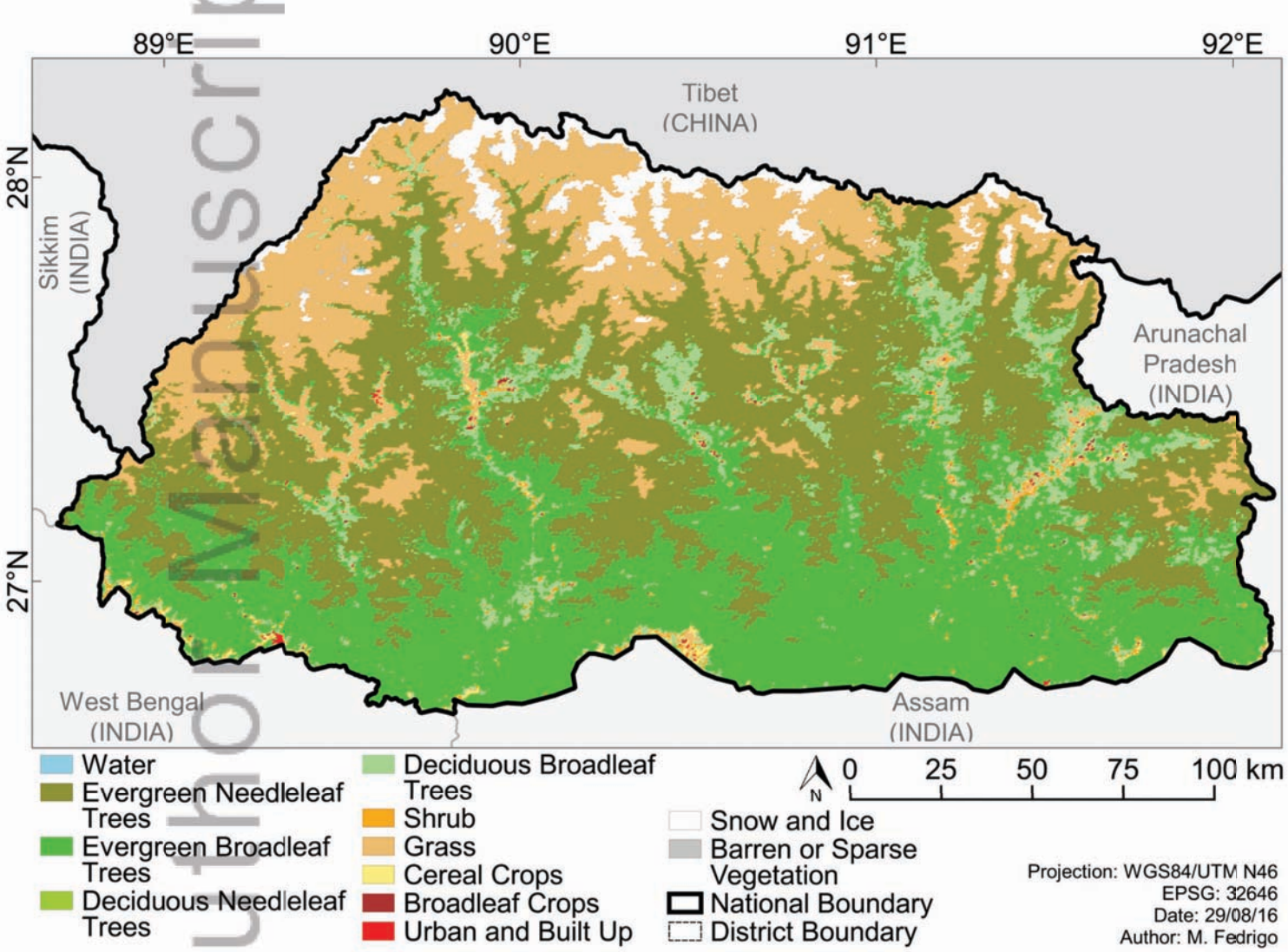

Figure3_LCC.tif

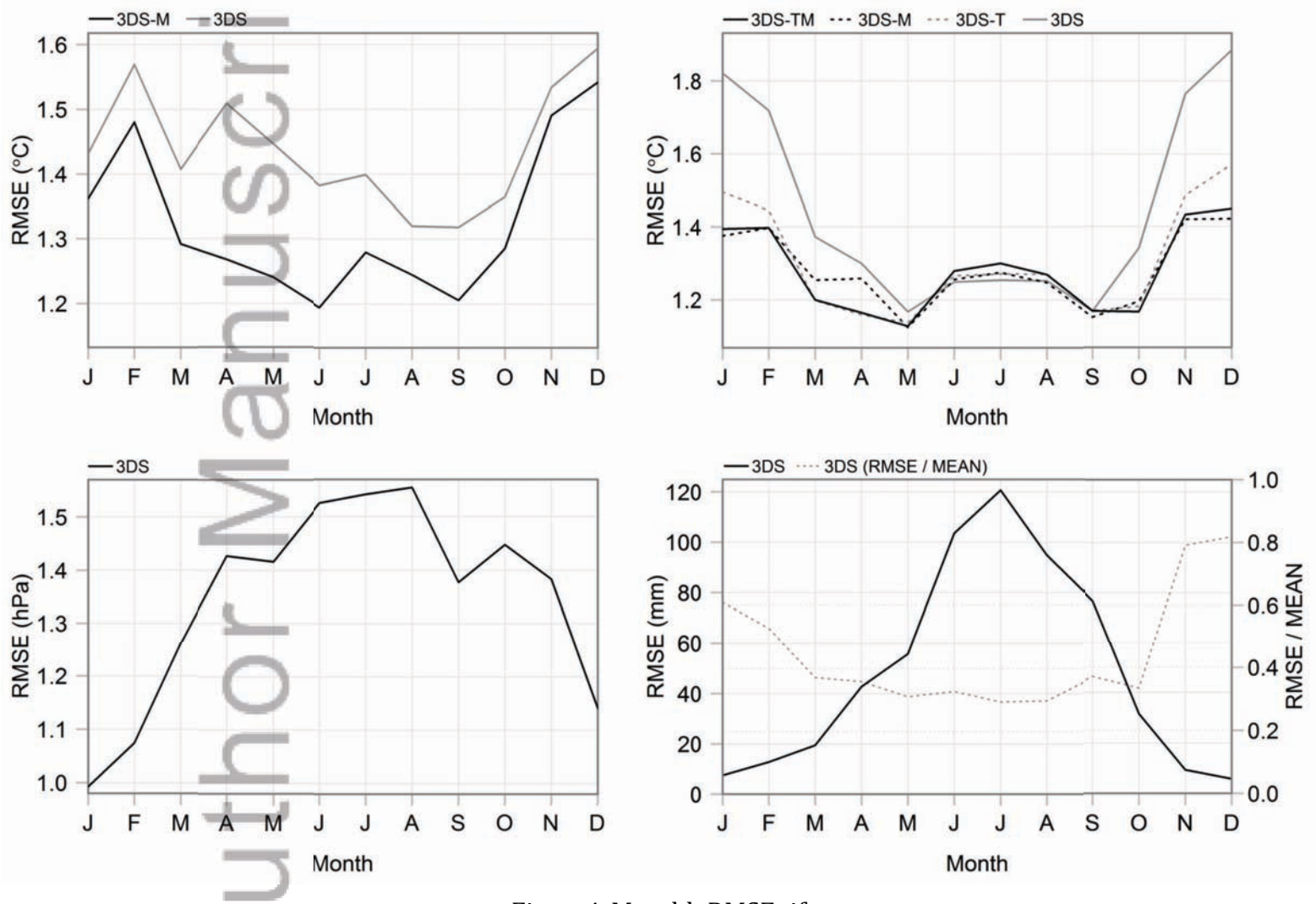

Figure4_MonthlyRMSE.tif

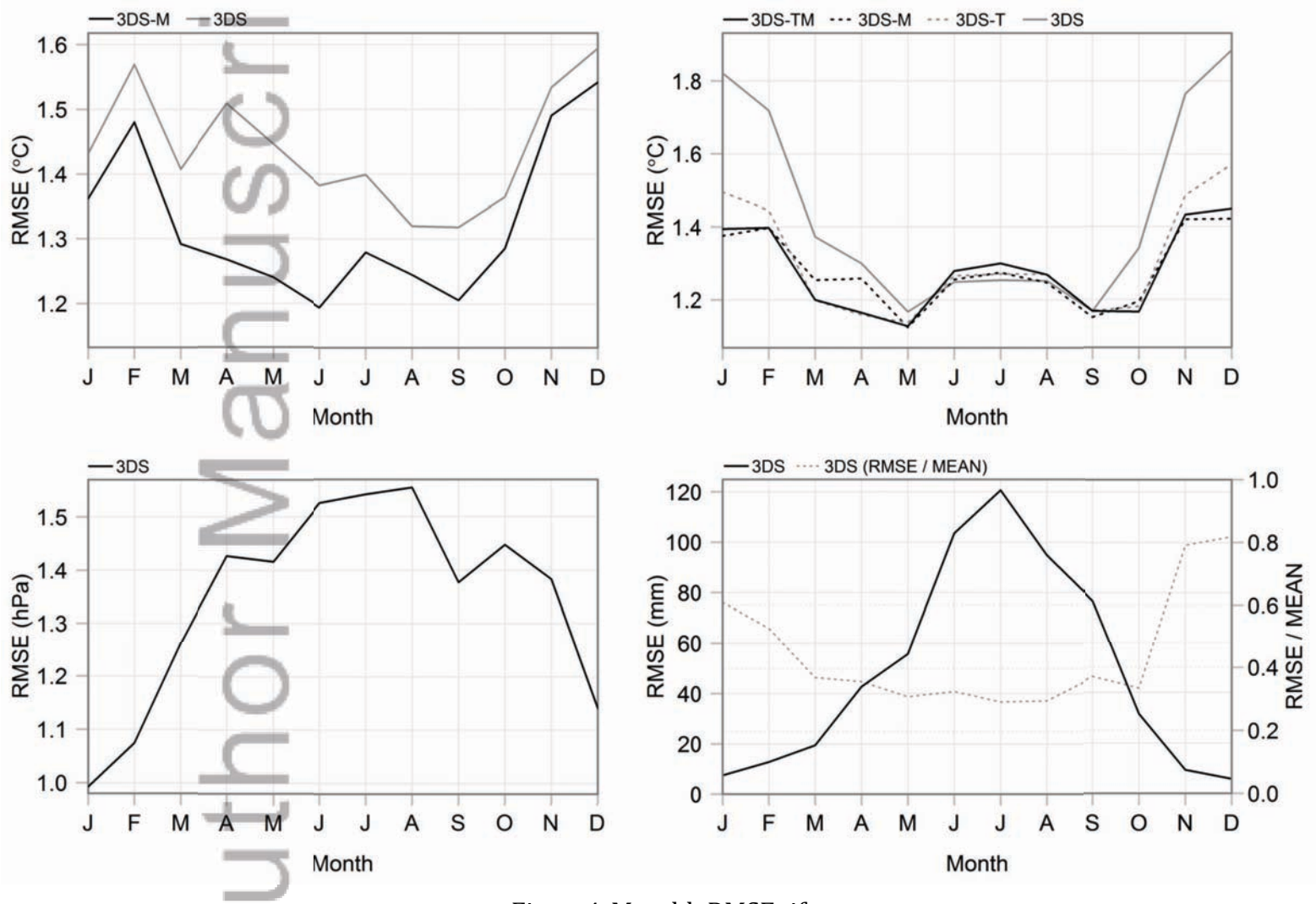

Figure4_MonthlyRMSE.tif

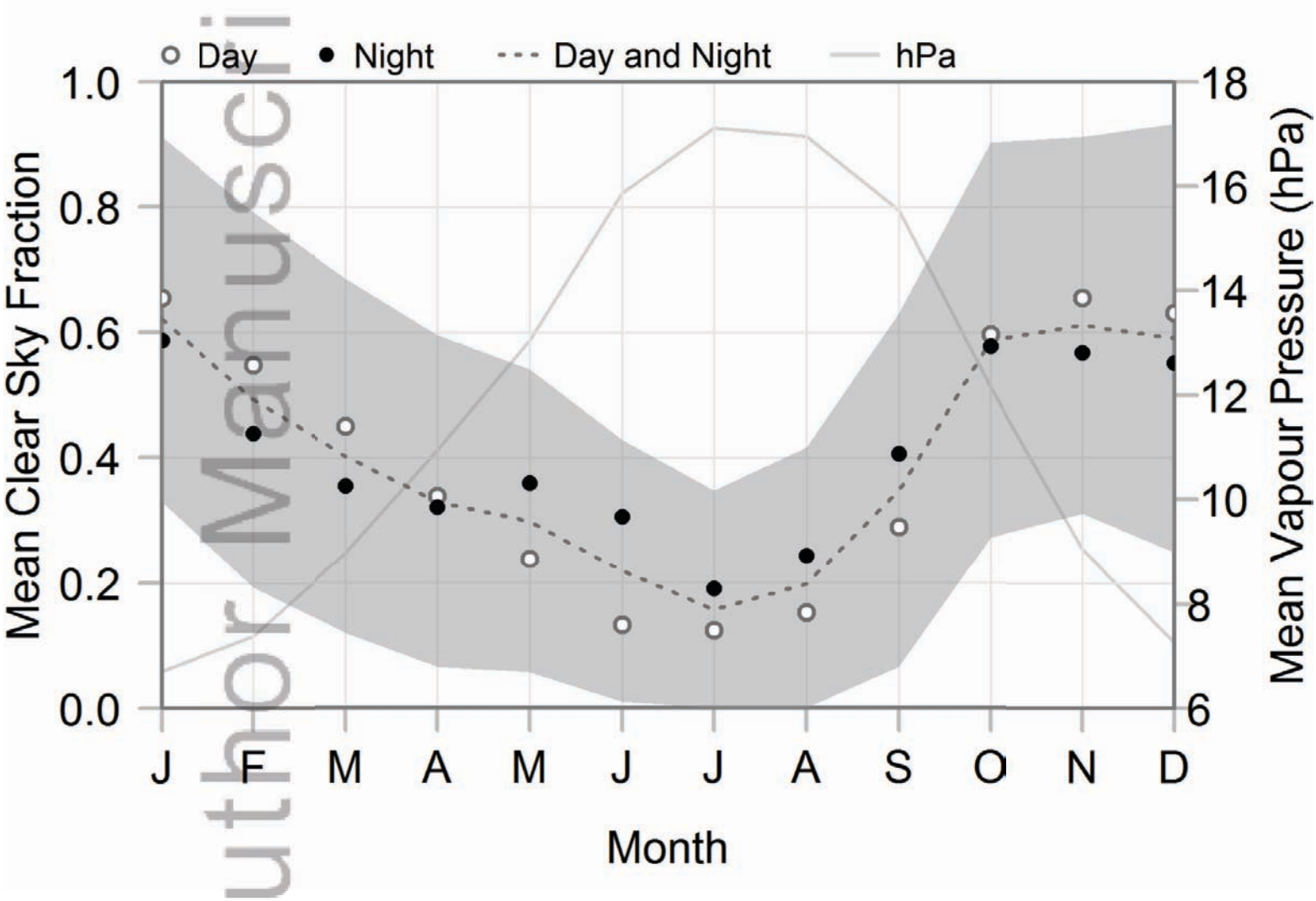

Figure5_ClearSkyVP.tif

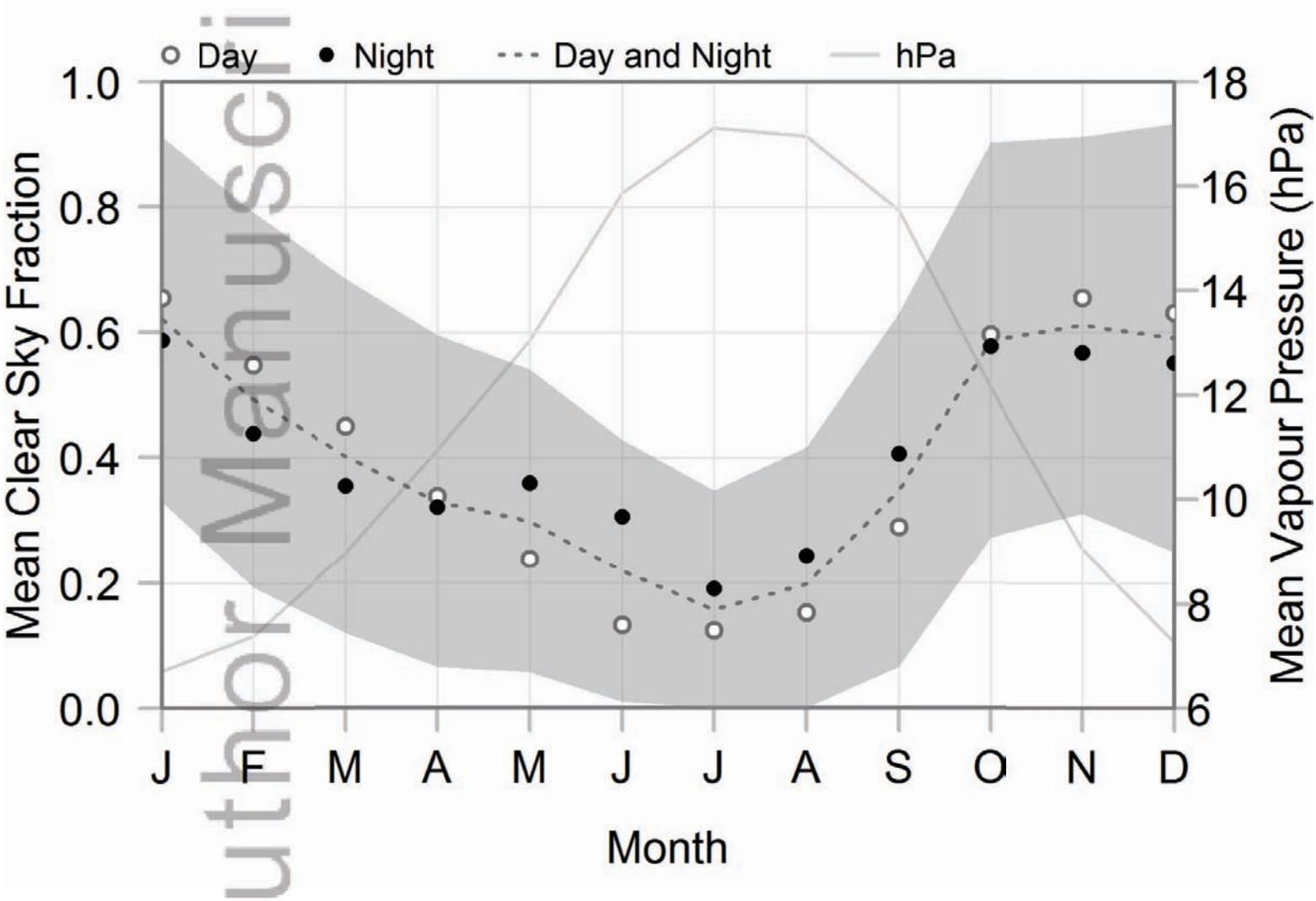

Figure5_ClearSkyVP.tif

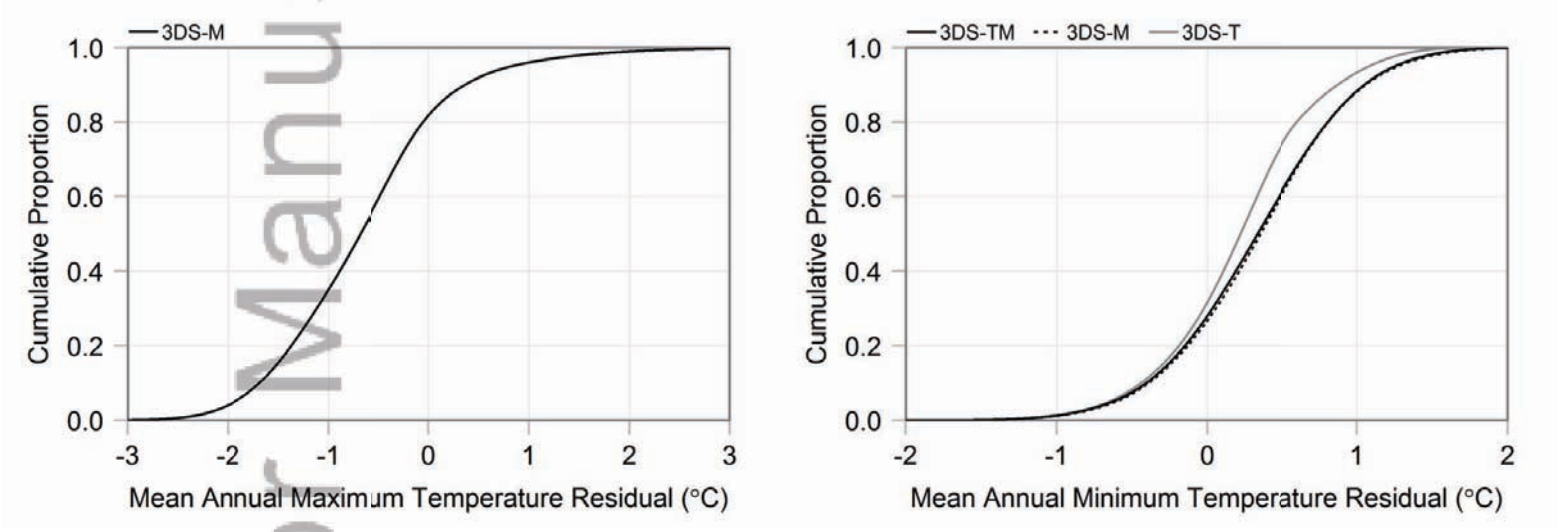

Figure6_ECDF.tif

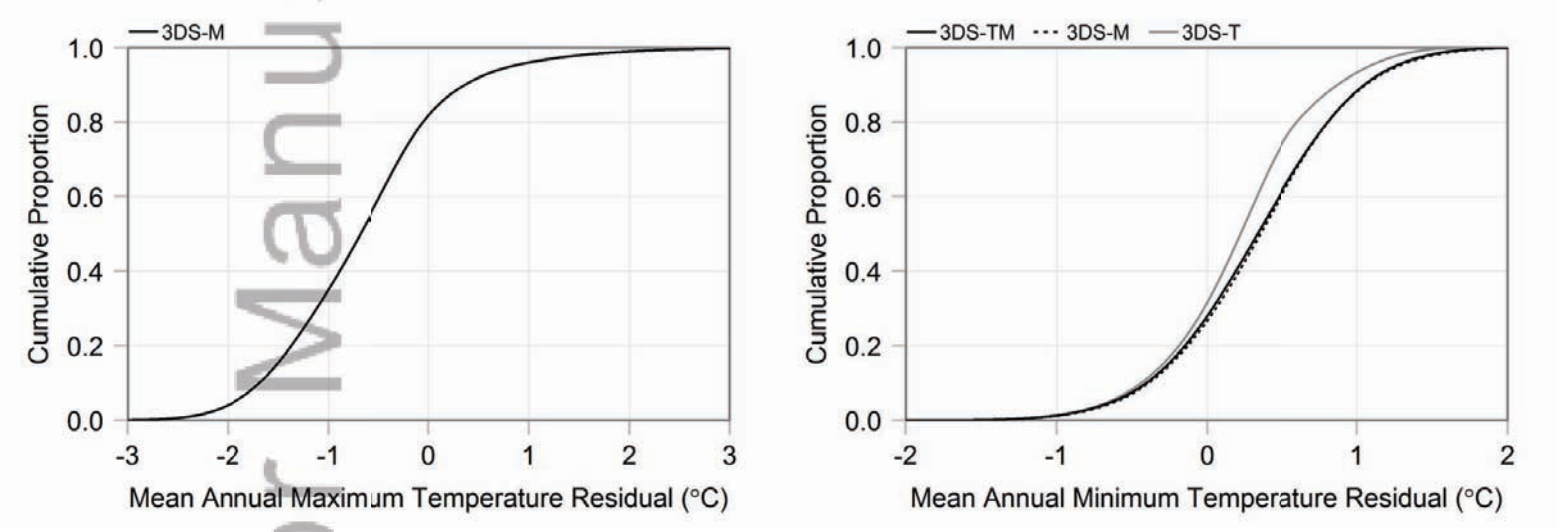

Figure6_ECDF.tif

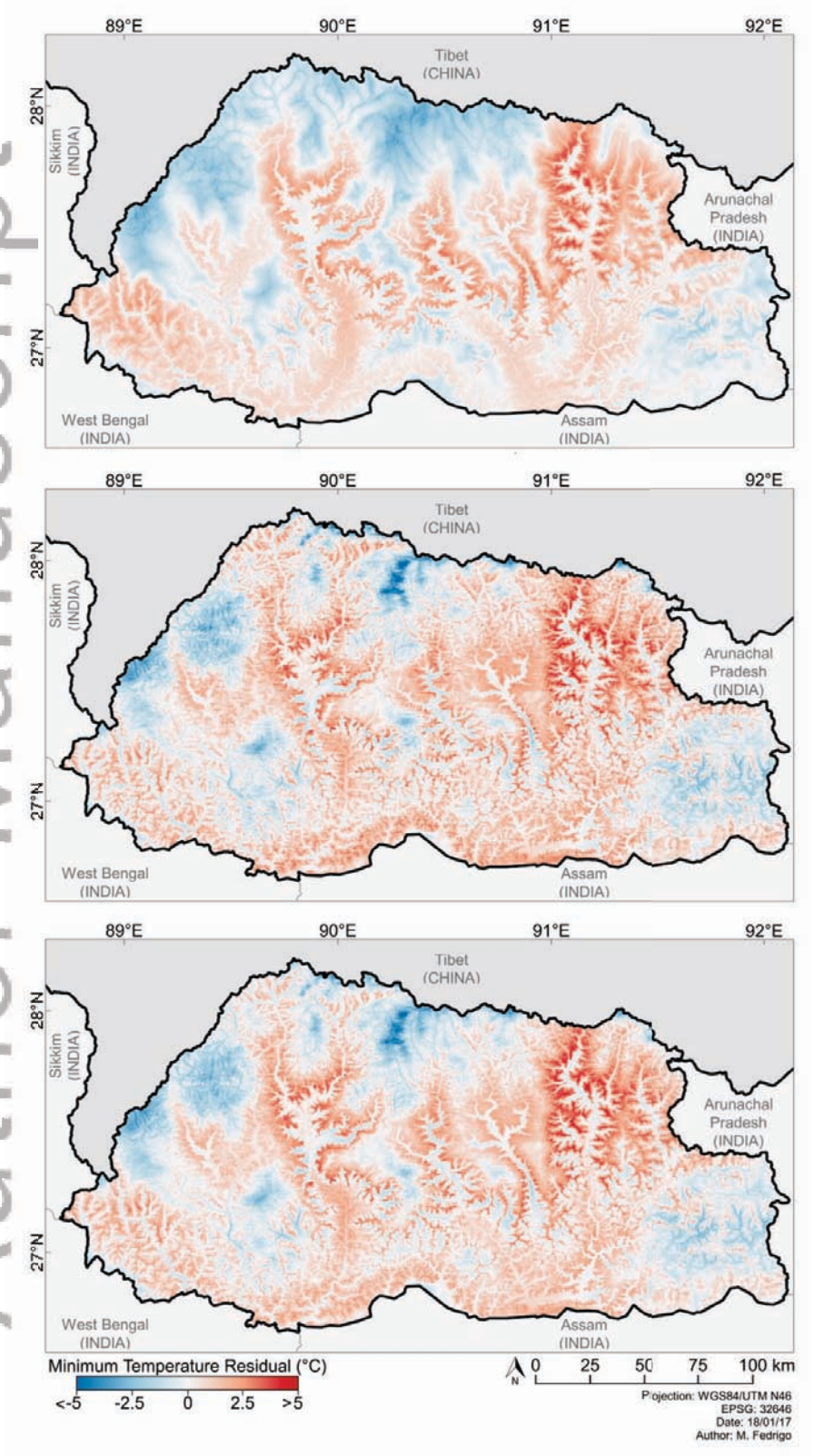

Figure7_MintResid.tif

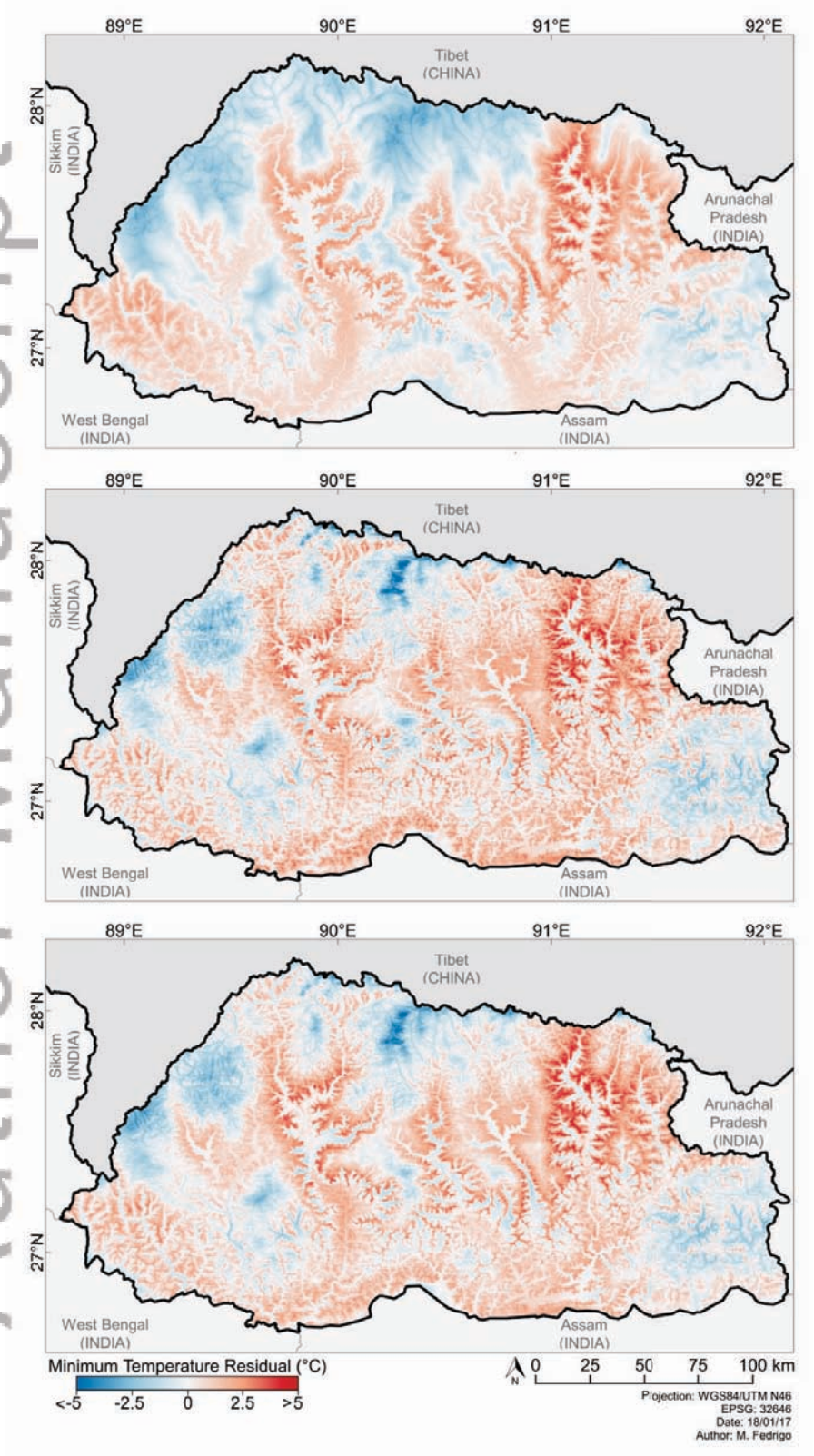

Figure7_MintResid.tif

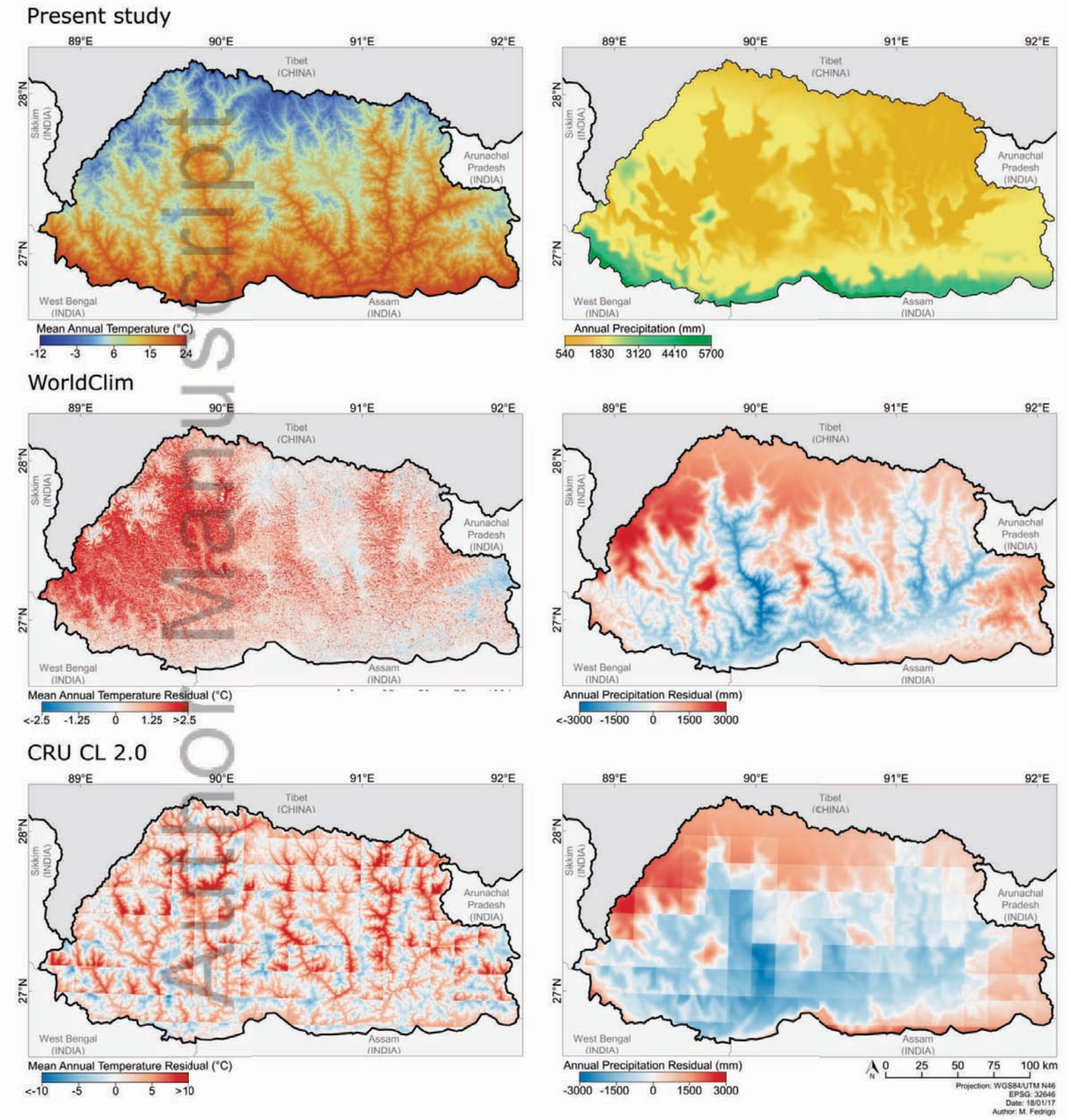

Figure8_MAT_MAP.tif

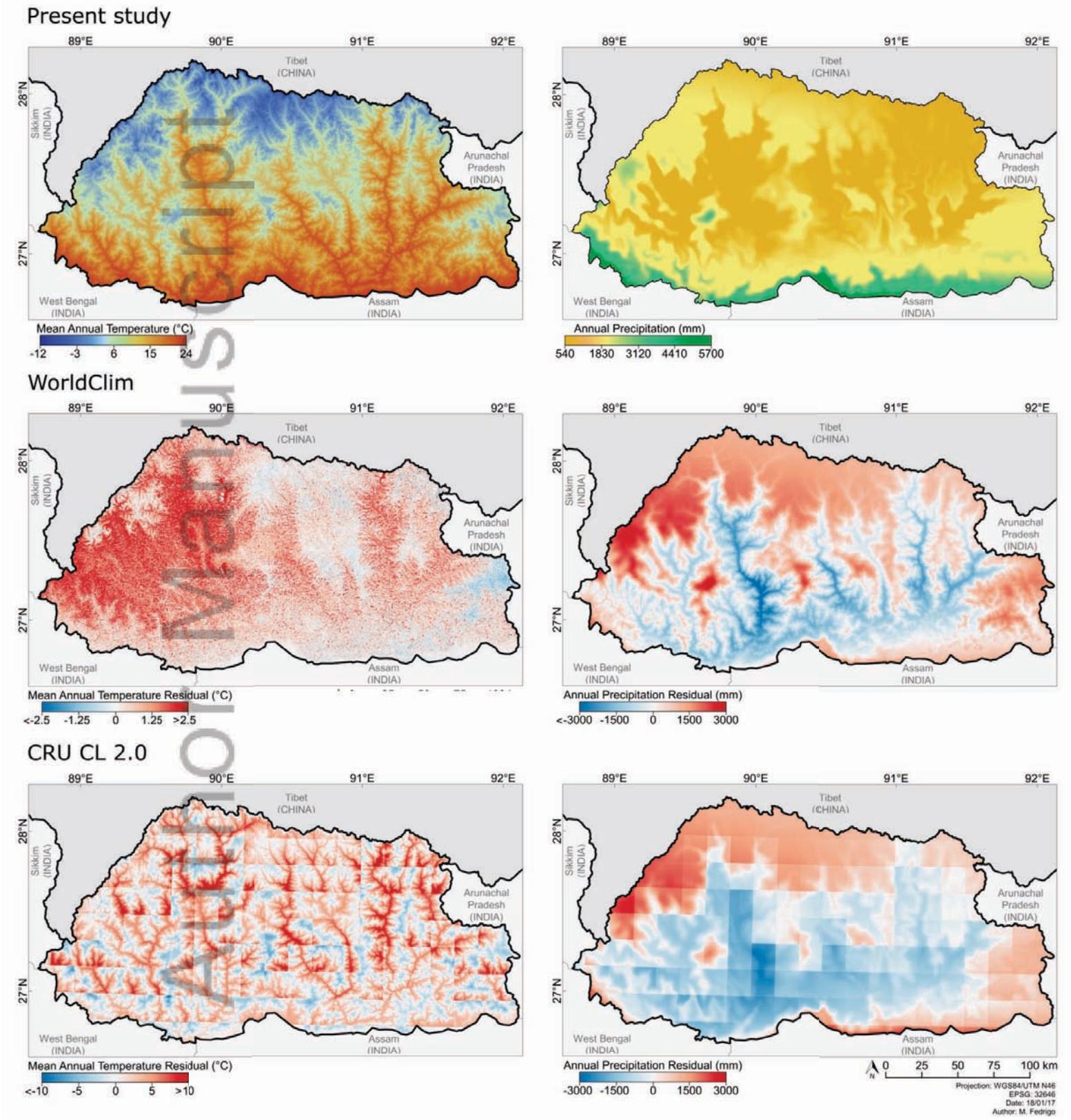

Figure8_MAT_MAP.tif